U.S. DEPARTMENT OF THE INTERIOR

U.S. GEOLOGICAL SURVEY

Concepts and Procedures Required for Successful Reduction of Tensor Magnetic Gradiometer Data Obtained from an Unexploded Ordnance Detection Demonstration at Yuma Proving Grounds, Arizona

by

Robert E. Bracken[1] and Philip J. Brown[1]

Open-File Report 2006-1027

[1]USGS, MS 964, Federal Center, Denver, Colorado 80225

Table of Contents

Abstract

On March 12, 2003, data were gathered at Yuma Proving Grounds, in Arizona, using a Tensor Magnetic Gradiometer System (TMGS). This report shows how these data were processed and explains concepts required for successful TMGS data reduction. Important concepts discussed include extreme attitudinal sensitivity of vector measurements, low attitudinal sensitivity of gradient measurements, leakage of the common-mode field into gradient measurements, consequences of thermal drift, and effects of field curvature. Spatial-data collection procedures and a spin-calibration method are addressed. Discussions of data-reduction procedures include tracking of axial data by mathematically matching transfer functions among the axes, derivation and application of calibration coefficients, calculation of sensor-pair gradients, thermal-drift corrections, and gradient collocation. For presentation, the magnetic tensor at each data station is converted to a scalar quantity, the I_2 tensor invariant, which is easily found by calculating the determinant of the tensor. At important processing junctures, the determinants for all stations in the mapped area are shown in shaded relief map-view. Final processed results are compared to a mathematical model to show the validity of the assumptions made during processing and the reasonableness of the ultimate answer obtained.

Introduction

Many geophysical applications rely on magnetic field measurements to discern characteristics of geologic source materials and buried objects. Typically, scalar data are acquired but may be converted to vector data as required by certain modeling routines. Vector components are derivable if the scalar data were acquired over a large surface with sufficient resolution. However, in unexploded ordnance (UXO) applications, where sources are nearby, there is a practical limitation to this approach (D.V. Smith, oral commun., 2004). Therefore, we consider vector-based acquisition methods.

Direct measurement of target-anomaly vector data is hampered by the huge Earth-field vector, which requires the attitude of the vector sensor to be recovered with practically unattainable levels of precision. For example, using the best available attitude-recovery systems along with a vector magnetometer, gives Earth-frame component accuracy to only about 5 nanoTeslas (nT). This problem is circumvented in tensor gradiometry, which incorporates the vector information without requiring such stringent knowledge of the sensor-array attitude.

Gradients are more useful for discerning nearby sources and source materials than are scalar or vector fields alone. Because gradient strength decreases with distance more rapidly than field strength, nearby sources are preferentially detected and distant sources are rejected. The tensor gradient can be manipulated to obtain source information through a number of methods that cannot be applied with fields only. One such method, called dipole mapping (Wynn and others, 1975), uses a tensor to find the location, depth, and moment of a dipolar source. Other methods involve the use of tensor invariants, which we briefly discuss herein (Pedersen and Rasmussen, 1990).

We performed a survey to demonstrate the effectiveness of a prototype tensor magnetic gradiometer system (TMGS) for detection of buried UXO. In order to achieve a useful result, we designed a data-reduction procedure that resulted in a realistic magnetic gradient tensor and devised a simple way of viewing complicated tensor data, not only to assess the validity of the final resulting tensor but also to preview the data at interim stages of processing.

The final processed map of the surveyed area clearly shows a sharp anomaly that peaks almost directly over the target UXO. This map agrees well with a modeled map derived from dipolar sources near the known target locations. From this agreement, it can be deduced that the reduction process is valid, demonstrating that the prototype TMGS is a viable geophysical instrument and that direct measurement of the magnetic gradient tensor is a reasonable data-acquisition mode.

This report shows how the demonstration survey data were processed and explains concepts required for successful TMGS data reduction. Although the procedures presented herein are applicable only to the prototype TMGS and to this particular data set, they serve as a vehicle for gaining a general understanding of the development and application of fluxgate tensor-magnetic gradiometer systems. They also form a solid

foundation for future choices of techniques and design modifications for this specific system.

Description of the Survey

On March 12, 2003, the U.S. Geological Survey (USGS) used the TMGS to perform a demonstration survey over a known UXO target at the Standardized UXO Test Site in the Yuma Proving Ground (YPG), Arizona . The target was a 60-mm mortar shell buried 0.25 m deep. We collected the data as 10-second stationary observations at five samples per second over a 3-m-square grid, called the "high-density grid," centered on the target and having 0.25-m grid cells. Smith and Bracken (2004) describe the survey in detail. Three categories of data were collected onsite: (a) primary measurements including tensor magnetics, gradiometer position, and gradiometer attitude; (b) spin-calibration measurements for the precise determination of a large group of calibration coefficients for the sensors and sensor array; and (c) thermal baseline measurements for correcting thermal drift in the sensors and sensor array. Some calibration data used in the reduction procedure were collected in the laboratory. The primary objectives of the survey were to show whether the TMGS could find the target UXO, to evaluate how well the target anomaly stands out against background noise, and to gain a feel for how accurately its location could be ascertained.

Description of the TMGS

Brief History: The TMGS was designed and built in the early 1990s for detection of volcano magnetic effects. These are time-varying magnetic fields produced in volcanoes by a variety of mechanisms (Zlotnicki and Le Mouel, 1988). The original instrument design required placement within about 3 km of expected volcanic events because gradients are preferential to nearby sources. In 1994 and 1995, the TMGS monitored near Kilauea Volcano, Hawaii and, after data-reduction, attained precision on the order of 0.25 nanoTesla per meter (nT/m) over periods of weeks to months (Bracken and others, 1998). However, over short periods of data collection, as would be applicable to UXO detection, the precision is expected to improve because long-period drift factors, which are difficult to remove, are not involved.

The original design specifications required that the magnetic sources (targets) be at least 25 m away from the sensor array, so that the gradients would remain nearly constant throughout the volume of the sensor suspension apparatus. However, for UXO detection, imaging, and discrimination, the sources will be much closer, resulting in significant gradient variation, or curvature, over the dimensions of the instrument. Therefore, in future redesigns, the sensor geometry and spacing will be appropriately modified to handle increased field curvatures. Additionally, the original design called for stationary measurements over long time periods. The UXO application requires a moving platform with measurements over short periods. Again, in future redesigns, the data-acquisition

circuitry and data-reduction techniques will be modified. Notwithstanding, the original design was used here to collect the data for this report.

The Physical Unit: The TMGS consists of two basic units: a tetrahedron that holds the magnetic sensors, called the tetrahedral em/mag sensor suspension apparatus (TESSA) shown in figure 1; and a cubical enclosure (called "Morris") that houses the magnetometer circuitry and data-acquisition systems (not pictured). TESSA is designed to maximize thermal and mechanical rigidity for reasons that will become clear later. Four tri-axial magnetic sensors, spaced 0.97 m apart, are placed at the vertices of the tetrahedron and are oriented in various attitudes that facilitate calibrations. Morris provides a thermally controlled environment (35°C) for the fluxgate magnetometer control circuitry. It also contains circuitry that measures the temperature of each sensor and samples the magnetometer output. The raw data are sent to a laptop computer for storage via an RS-232 link.

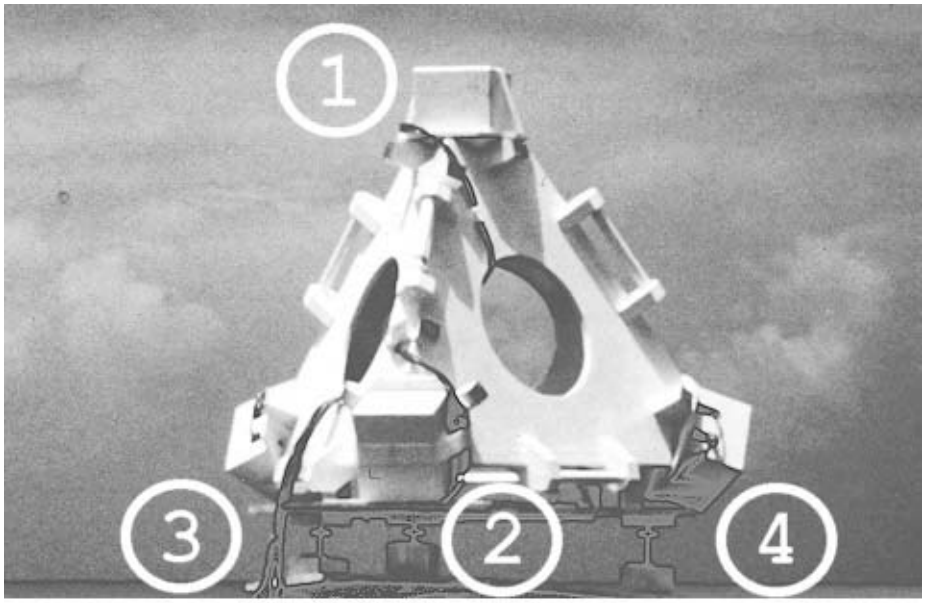

Figure 1. TMGS sensor array (TESSA) with sensors numbered.

Currently, all data reduction occurs in postprocessing. However, the reduction procedures of future designs will most likely be carried out in real time on the laptop computer. This would provide an immediate readout of user-interpretable tensor derivatives, as well as downloadable files ready for analysis and archiving.

The Magnetic Field

The UXOs that are detectable by the current TMGS design produce a static magnetic field. That is, the field does not vary as a function of time; or at least it varies so slowly

that Maxwell's magnetostatic equations are practically satisfied. The magnetic field is a vector field, meaning that it has both magnitude and direction. It is also a potential field, meaning that it can be described as the derivative of a potential function and thus, it obeys Laplace's equations. All of these qualities provide mathematical bases and constraints for analyzing magnetic sources, and hence, UXO targets. In other words, the magnetic anomaly produced by a particular UXO contains useful information about that UXO.

Magnetic Sources: The source of the field is magnetization, within the target, of both induced and remanent (permanent) varieties. It should be noted that both forms of magnetization passively exist within the source material, and are not generated by active signals from the TMGS. The induced magnetization is caused by and proportional to the geomagnetic field. In earth materials, which have relatively low susceptibilities, the magnetization is also generally aligned with the field. However in high susceptibility materials, such as UXO, the direction of induced magnetization is difficult to predict due to complicated boundary conditions. Remanent magnetization, on the other hand, is independent of the Earth's field and can have essentially any orientation and magnitude.

The smallest irreducible source of magnetic field is a magnetic dipole at the atomic level, and magnetization is a volumetric distribution of dipoles. We assume that dipoles are aligned throughout the target, which produces a net dipole moment together with a number of higher order moments. The suite of moments will be indicative of the distribution of magnetization, which in turn is controlled by the composition, shape, and distribution of materials within the UXO target.

Therefore, by appropriately measuring the magnetic field at any point or set of points outside the source, characteristics of the magnetization can be ascertained, including its location (relative to the sample points) and possibly aspects of its distribution (within the UXO). Further analysis of the magnetization may yield specific information about mass, dimensions, orientation, and the like. However, it must be stressed that magnetization can vary widely among individuals of a given type of UXO, creating a likelihood of non-uniqueness and overlapping characteristics among differing types. Moreover, the magnetic field itself, no matter how precisely measured, does not uniquely determine the distribution of magnetization, much less the shape and size of the source material. Nevertheless, statistical analysis of magnetization distributions may provide a basis for determining probabilities for classification of UXO (Billings, 2004).

Superposition: In practice, the field being measured is a combination of magnetic fields produced by a number of sources, both nearby and distant and both small and large. The observable field at any point in space and time is actually the vector sum of all the contributing fields at that point. This principle is called superposition, and it is simply a statement that magnetic fields combine linearly, and that their combining can be described mathematically as a linear operation. This principle has bearing on instrument design and data reduction.

An isolated measurement of magnetic field (at a particular location and a particular time) does not contain any information that identifies or separates its component fields. However, by taking multiple measurements, separated by space and (or) time, certain component fields can be separated and identified. This can be done if each field varies according to a unique and identifiable spatial and (or) temporal function.

It can therefore be assumed that any magnetic field measurement will be a sum of several different fields, originating from differing sources and having differing characteristics. Some of these component fields will be of interest; the rest must be removed. The separation and removal of undesirable fields is done by specialized instrumentation, data acquisition and reduction, and interpretation methodologies that take advantage of unique and identifiable aspects of the superpositioned fields through multiple measurements taken over spans of length and time. (Some of these methods and the fields they handle are mentioned in the next few sections.)

The TMGS is an example of this type of specialized instrumentation. Each sample is a set of simultaneous measurements that are spatially separated. Then, samples can be taken at a prescribed sample interval, during which time the instrument can be stationary or in motion. Thus, the TMGS is a tool for separating magnetic fields by looking at both spatial and temporal variations.

The job of separating fields includes the requirement of being able to measure small fields that have been added to large fields. For example, the Earth's field is several orders of magnitude larger than the typical target anomaly; this predicates having instrumentation with a large dynamic range that can measure tiny variations riding on a huge signal. The magnetometers used in the TMGS have a dynamic range approaching 140 decibels (dB), which, imagining magnetic fields to be analogous with sound, makes them about 1,000 times quieter than a home stereo CD player. More important, this range allows the TMGS to preserve the tiny signals from UXO targets while rejecting a huge common-mode signal from the Earth’s field, as will be discussed later.

Scalar Field Measurements: The most common magnetometers in use today measure only the magnitude of the field and are insensitive to its direction. This measurement is useful primarily because the target's field is much smaller than the Earth's field, making the direction of the sum of the two fields nearly the same as the Earth's field. Consequently, most geophysical applications treat the magnetic field as a scalar quantity with its resultant simplifications. However, except under ideal circumstances where the scalar field is accurately known over an effectively infinite surface, scalar measurements loose the vector direction information of the target's field.

Nevertheless, the target's anomaly often can be distinguished spatially from other anomalies and fields because measurements are taken at many locations. Also, temporal fields, such as the diurnal variation, can be removed by collecting base magnetometer data at a nearby stationary location. In spite of these techniques, distant sources can add

noise and uncertainties to measurements of nearby targets, and multiple nearby targets can become indistinguishable from one another.

Scalar Gradient Measurements: Because the magnetic field varies from place to place, it is appropriate to consider direct measurement of that variation. Operating two or more scalar magnetometers at a fixed distance apart produces a scalar gradient measurement, which is the spatial rate of change of the field magnitude in the direction of the baseline between the two measurement points. The gradient is preferentially sensitive to nearby sources because, while the magnitude of a dipolar field is proportional to the inverse cube of the distance to the source, the dipolar gradient goes by the inverse fourth power. Therefore, gradient measurements improve the spatial separation of anomalies, essentially eliminate interference from distant sources, and obviate the need for a base magnetometer.

The scalar gradient has an associated direction, which depends on the orientation of the baseline between the two scalar magnetometers. By constructing a 3-axis scalar gradiometer (one with three independent gradient baselines), three of the five independent components of a gradient tensor can be found, assuming the direction of the total field is known by an independent means. This information is also helpful in separating anomalies and modeling nearby sources, but it does not form a complete characterization of the magnetic field.

Vector Field Measurements: A vector magnetometer measures both the magnitude and direction of the magnetic field, as contrasted to the scalar magnetometer that is insensitive to direction. (Here, the direction is that of the magnetic field lines, not the baseline direction as in the scalar gradiometer.) Complete measurement of the vector field requires three simultaneous linearly independent measurements. This is the same as three different axis directions; hence the name, "tri-axial vector magnetometer." If these axes are coincident and orthogonal (as in the rectilinear coordinate system with x, y, and z axes), then they represent the three components of the magnetic field vector, called b_x, b_y, and b_z. The field magnitude is then the square root of the sum of the squares of the three components, and the field direction is defined by the direction cosines. Of course, both the location and the precise attitude of the vector magnetometer must be known in order to define the field. The TMGS is based on vector field measurements.

Magnetic Gradient Tensor Measurements: If vector field measurements are simultaneously made at two points in space, then three gradient quantities are obtained. They are the rates of change of each of the three magnetic field components (b_x, b_y, b_z) as functions of distance in the direction of the baseline between the two measurement points. For example, the gradient of the y component of the magnetic field in the x baseline direction is expressed as the partial derivative, $\partial b_y/\partial_x = g_{yx}$. Of course there are three magnetic field directions; but there are also three possible baseline directions, resulting in nine gradients. These nine gradients are arranged into a 3-by-3 matrix, a

mathematical object called the magnetic gradient tensor. It is symbolically written in row and column format as:

$$G = \begin{bmatrix} \partial b_x/\partial x & \partial b_y/\partial x & \partial b_z/\partial x \\ \partial b_x/\partial y & \partial b_y/\partial y & \partial b_z/\partial y \\ \partial b_x/\partial z & \partial b_y/\partial z & \partial b_z/\partial z \end{bmatrix} = \begin{bmatrix} g_{xx} & g_{yx} & g_{zx} \\ g_{xy} & g_{yy} & g_{zy} \\ g_{xz} & g_{yz} & g_{zz} \end{bmatrix}$$

Maxwell's magnetostatic equations require that both the curl and the divergence of the magnetic field be equal to zero in a sourceless region (Kaufman, 1992). This means that the gradient tensor will be symmetric and its trace components will sum to zero. In other words, only five of the nine tensor components are independent. This has implications that simplify and improve TMGS sensor design, noise characterization, data reduction, and interpretation.

At a point in space and time, the magnetic gradient tensor together with the three vector field components, consists of a complete description of the magnetic field to the 1st order. That is, the TMGS directly measures 0th- and 1st-order spatial derivatives, but not 2d and higher order spatial derivatives.

Important Concepts as Applied to the Prototype TMGS

At the practical level, magnetometers and magnetic systems are found to have imperfections and deviations from the ideal that necessitate corrections and compensations in data reduction processes. Of course, the development of any system strives toward the theoretical and the ideal. But in the physical device, the greatest attention must be paid to providing predictable behavior, stability, and repeatability within the narrowest limits of precision, while deferring corrections and compensations for accuracy to subsequent data-reduction processes. The output of the physical device can then be moved toward the theoretical and the ideal by applying knowable though not ideal parameters of the physical system in mathematical reductions. Consequently, proper identification of system parameters is critical to obtaining valid results and is possibly the most important aspect of developing a data-reduction procedure for the TMGS.

For example, the Narod Ring Core magnetometers used in the TMGS are among the finest tri-axial fluxgates in the world. They are designed after the MAGSAT vector magnetometers (Acuna and others, 1978), and USGS magnetic observatories use them for reporting of the official HDZ vector data (Narod, 1987). Their output is precise and repeatable, yet no axes are perfectly orthogonal. Consequently, if the data reduction does not “know” and apply the relative axis-angle parameters—if it blindly assumes that the axes are orthogonal—then the resulting tensor will be erroneous. There are a number of subtleties like this one that the data-reduction procedures must take into account, and we must understand why these subtleties exist. Hence, this section on important concepts is provided.

Extreme Attitude Sensitivity: Vector magnetometers in the Earth's field are extremely sensitive to attitude variations. For example, if an axis of a vector magnetometer is oriented approximately perpendicular to the Earth's field and then its attitude is changed a slight amount, moving the axis, say, 20 micro-radians (μr) or 4 arc-seconds toward the Earth-field vector, then the axis will read an increase of 1 nT. Conversely, if the same axis will detect a 0.01-nT change in magnetic field, then it will also detect a 0.2-μr or 0.04-arc-second change in attitude. Therefore, a vector magnetometer, such as is used in the TMGS, is like a high-precision tilt meter, returning attitude information relative to the direction of the magnetic field vector with precision down to 0.2 μr.

If the intent is to measure magnetic-field components, the magnetometer's attitude must be known from an independent source with extremely high precision. Unfortunately, the best inertial guidance systems track attitude relative to a geographic reference frame only down to about 100 μr. If this level of precision was applied to vector measurements in the Earth's magnetic field, the attainable precision would be about 5 nT.

Considering that the field from a 20-mm UXO may be on the order of 5 nT at a range of 0.5 m, it can be concluded that the vector components of such a UXO cannot even be detected above the noise generated by attitude uncertainty, much less be modeled. This leads us to the idea of mechanically locking two (or more) sensors together. In this configuration, one sensor can be thought to act as a high-precision reference that tracks the attitude variations relative to the Earth's field, while the other measures residual variations. However, we quickly see that, in a realizable system, no particular sensor will be removed far enough from the nearby sources to act as a pure Earth-field reference, nor do the residuals measure components of the magnetic field. Instead, by mechanically locking sensors together and differencing them, we obtain spatial gradients; two or more vector magnetometers affixed to a rigid platform become a magnetic gradiometer.

Common Mode and Angular Stability: When the gradient is calculated, differencing removes any signal that is common to both magnetic sensors. (Normalizing this difference with respect to spatial separation yields a gradient.) In this case, the Earth's field is by far the largest common field and therefore correlates between both vector magnetometers, producing huge common-mode signals among their various components. The common-mode signals from either magnetometer are then several orders of magnitude greater than any of the gradient-producing signals. This dynamic range puts rigorous demands on the gradiometer to maintain a precision balance between the magnetometers while the platform undergoes angular motion, mechanical shock, and thermal variation during data collection. The precision balance may also be called tracking and has to do with the ability of readings from one magnetometer to track precisely with readings from the other.

One aspect of tracking involves angular stability, which equates to minimization of mechanical and thermal deformation. It was shown above that the attitude of a vector magnetometer needed to be known to about 0.2 μr, relative to a geographic reference

frame. Now in the gradiometer configuration, the same figure applies, but it is relative to the other sensor instead of the geographic frame, assuming that a gradient is the desired quantity. While the geographic reference frame cannot be ascertained with sufficient precision, the attitudes of magnetometers in a gradiometer configuration can be maintained relative to one another to better than 0.2 μr. However, maintaining this level of stability challenges both the mechanical and thermal characteristics of materials and geometries used in the sensor suspension apparatus (SSA), or platform.

The difficulty in achieving sufficient angular stability serves to illustrate the huge effect of the Earth's field and is part of the pervasive issue of common-mode field rejection, which is of foremost importance and drives much of the gradiometer design and processing methodology.

Gradient Measurements: The magnetic gradient tensor is derived by taking the difference between magnetic vector measurements and normalizing by the separation distance. (Devices that intrinsically measure gradients are not available.) Because of the Earth's large field and the common-mode signals it produces in the gradiometer, it is of paramount importance that the magnetometer sensors be locked together by a suspension apparatus that minimizes relative temporal angular variations, whether due to thermal expansion or to mechanical strain. In the current design, the tetrahedral shape of TESSA balances these microscopic movements so that the net relative angular variations are minimized while providing the largest possible baseline for gradient sensitivity. The tetrahedron is a mechanically stable geometry because stresses are transmitted primarily along the edges (line segments separating the vertices), so that strains become mostly compressional or extensional, and not flexural. The symmetry helps minimize thermal angular changes because as the ambient temperature changes, all six edges will expand or contract by similar amounts. Meeting this angular-stability criterion together with the high quality of the magnetometers makes it possible to measure the magnetic gradient tensor.

Simultaneous Measurement: The current configuration of the TMGS has 4 tri-axial magnetic sensors, each with 3 axes, which makes a total of 12 vector field axes. After differencing of these 12 axes, there are 6 gradient baselines, only 3 of which are linearly independent; and this leads finally to 9 measured gradients. The key point here is that the 12 vector field axes are sampled simultaneously during data collection, while the gradients are derived from the vector field data through subsequent data-reduction procedures.

Rejection of Motion-Related Common-Mode Signal: Simultaneous sampling becomes critical when data are being collected on the fly. The platform yaws, pitches, and rolls, which leads to angular rates of change and, hence, higher frequency content in the common-mode signals. (The common-mode signals have their common modality among the 12 vector field signals by virtue of the fact that all 12 signals have most of their amplitude originating from the common magnetic field, which is the Earth's field, and most of their variation due to angular rates of the platform in that field.) The higher

frequency content implies rapid variation of signal amplitude. Consequently, if the signals were sampled sequentially instead of simultaneously, then there would be opportunity for a time-varying common-mode signal to have a different value on each axis. This would irreversibly mix temporal variations in with the spatial variations, defeating the spatial gradient measurement. Conversely, if the signals are sampled simultaneously, temporal variations are rejected, being separated and removed from the spatial measurements.

However, simultaneous sampling is only part of the picture. Before sampling occurs, the magnetic field must first be converted to a measurable electrical signal by the magnetometer. The conversion effectively imposes a series of linear processes, or filters, that can be characterized by a transfer function that most likely will not have a flat spectrum nor zero-phase at all frequencies. Therefore, truly simultaneous measurements at all applicable frequencies can only be achieved by balancing the transfer functions among all of the axes on all of the magnetometers. Any application from a moving platform mandates this balancing procedure, which is required to ensure that the magnetometers will track precisely.

Nevertheless, transfer-function balancing was not an essential data-reduction step for the data collected in the high-density grid because the platform was brought to rest at each station before sampling commenced. Consequently, further description is not included in the processing description to follow.

Rejection of Diurnal and Other Geomagnetic Variations: Most forms of common-mode signal, other than those generated by attitude variations, are slowly varying, such as diurnal variations; for these, precise tracking is not as critical. Although they are normally a menace to magnetic field measurements, they have no effect on the gradients because of common-mode rejection. This, however, does not mean that a gradiometer can be used successfully in severe geomagnetic storms because high magnetic activity can cause temporal ground currents and secondary fields that may appear as nearby sources. Furthermore, a tri-axial base magnetometer should always be used in conjunction with TMGS surveys to remove temporal variations from the vector-field portion of the data.

Slowly Varying with Attitude: While the vector field components are extremely sensitive to attitude variations, the gradients (components of the gradient tensor) are only mildly sensitive. Therefore, if the objective is to locate a magnetic source having a field that is small compared to the Earth's field, then the attitude recovery system for a vector magnetometer must be far more precise than that of a tensor gradiometer doing an equivalent job.

As an illustrative example, start with a purely dipolar source oriented perpendicular to the Earth's 50,000-nT field and having a field strength of 8 nT along its 0.5-m equatorial radius. Establish an observation point at one of the two intersections of its 0.5-m equatorial radius and the Earth-field line that runs through the dipole. Now at the observation point, the dipole's field is 8 nT and runs perpendicular to both the Earth's field and the dipole's equator.

The total field strength is 50,000.00064 nT and the field direction is 160 μr (33 arc-seconds) from the Earth-field direction. Therefore, if a vector magnetometer was associated with a state of the art attitude recovery system (with a precision of 100 μr) it would barely be able to sense the presence of the dipole from this observation point, showing its field strength to be somewhere in the range of 3 to 13 nT, or an error of 62.5 percent of the full dipolar field expression.

On the other hand, one of the gradients at the observation point ranges from –48 to +48 nT/m depending on its baseline direction. If the same 100-μr attitude precision is applied to a gradiometer, then the greatest expression of gradient error is in the range of ––0.0048 to +0.0048 nT/m, or an error of 0.01 percent of the full gradient expression. In this instance, the vector magnetometer is over 6,000 times more sensitive to attitude recovery error than the gradiometer. Therefore, with a nominal attitude recovery system, the TMGS is able to provide better data than a vector magnetometer using state-of-the-art attitude recovery. The gradiometer's mild sensitivity to attitude is also a useful concept that has application to thermal corrections.

Preferentially Sensitive to Nearby Sources: As previously described, gradients respond to nearby sources and tend to reject distant sources. Of course, this is why a tensor gradiometer is ideally suited for UXO work. Keeping this in mind, it becomes clear that in areas having magnetic materials near the surface, it is better to have an increased standoff (sensor height above the surface) to keep the surface magnetic signatures from swamping the UXO.

Leakage of the Earth's Common Mode Field into Gradient Measurements: Assuming that, as alluded to above, (a) the magnetometers are quiet and stable, (b) the platform has minimized angular instabilities, and (c) the axis tracking errors can be removed, then the instrument is qualified to acquire gradient-tensor data. At this point, data-reduction procedures become important. This section describes the first of the subtleties, mentioned previously, that results from imperfections and deviations from the ideal and that requires application of system parameters in mathematical reductions.

This subtlety is a leakage of the Earth's common-mode field into the gradients. It is caused by slight differences among the magnetometers, such as small disparities in calibrations, sensor axis inorthogonalities, and sensor attitude misalignments. All of these things can be corrected in data reduction, given accurate knowledge of the governing system parameters. For example, the relative attitudes of the sensors must be known precisely in order to align them mathematically.

The leakage phenomenon is best described by way of an example that reflects typical TMGS behavior. Suppose that two truly parallel axes are being differenced for a gradient calculation as shown in figure 2. There is no gradient present, and the field difference between the axes correctly indicates a zero gradient both before and after the gradiometer is rotated one degree toward the Earth's field vector. Suppose now that the two axes are

one degree out of parallel as shown in figure 3. If gradient calculations are made, errantly assuming the axes to be parallel, then systematic errors, or false gradients, will appear. More insidiously, the false gradients will vary with sensor-platform attitude. Figure 3 shows a platform rotation artifact that could falsely be interpreted as a 10-nT/m anomaly.

This false anomaly is more than ample to swamp a real anomaly from a small UXO target. Furthermore, the false gradient is correlated to TESSA's attitude and is entirely a manifestation of common-mode leakage. In fact, any gradient reduced with incorrect parameters will likely have 2 or 3 times bigger errors because of similar effects compounded from calibration disparities, axis inorthogonalities, and attitude misalignments.

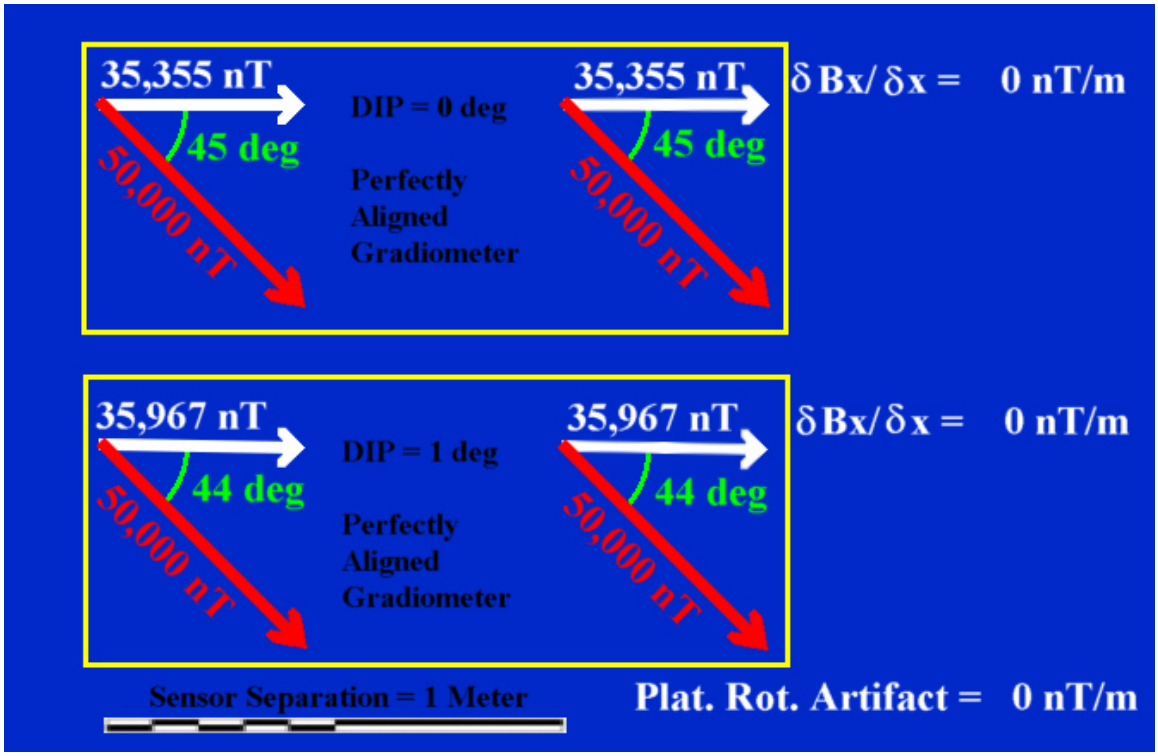

Figure 2. An example of a gradiometer with no common-mode leakage. The sensor axes are parallel, and the sensor platform (the yellow box) is shown in two different attitudes relative to the earth's main field vector. There are no false gradients and no platform rotation artifacts.

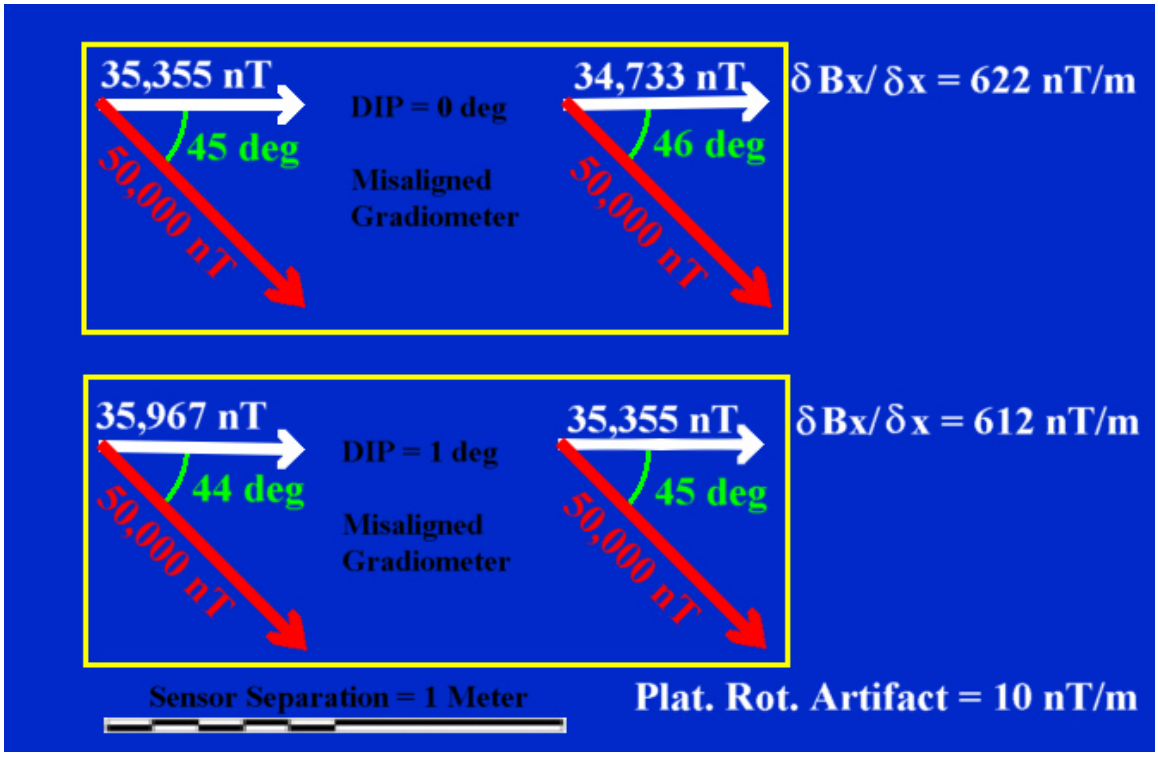

Figure 3. An example of a gradiometer with common-mode leakage in a zero-gradient space. The sensor axes are misaligned by one degree, and the sensor platform (the yellow box) is shown in two different attitudes relative to the Earth's main field vector. There are false gradients of 622 nT/m and 612 nT/m; and a platform rotation artifact, or false anomaly, of 10 nT/m.

Common-mode leakage is reduced to tolerable or insignificant levels by introducing coefficients derived from a special procedure, called spin calibration, which will be described later. If the calibration coefficients are not used, or incorrect calibration coefficients are used, the resultant tensor will be correlated to undulations in the ground surface and will bear no resemblance to any target anomaly or gradient.

Thermal Drift: The magnetometer sensors used in the TMGS have a certain amount of temperature-dependent drift. Certain of the magnetometer calibration coefficients are actually functions of temperature, and should have been derived as such. However, time and facilities at YPG allowed only the constant portion of the coefficient functions to be measured.

Another contributor to thermal drift is differential expansion of TESSA. If one side is exposed to solar heating, it will tend to expand more than the shaded side. This will tend to alter the measured gradients as the sensor attitudes change differentially in the Earth's field, as illustrated in figures 2 and 3. According to Bracken and others (1998), data taken in Hawaii showed that TESSA produces angular thermal drift of less than 0.05 nT/m per degree Celsius, when completely shaded. However, while collecting the high-density grid

data, differential heating may have been a bigger factor because of direct sunlight on the face defined by sensors numbered 1, 3, and 4 (fig. 1), which was facing south. The future design of the sensor suspension apparatus, which will be specific for UXO work, is expected to improve substantially upon the tetrahedron in minimizing angular thermal drift.

The technique used for reducing thermal drift in the high-density grid data removed both coefficient and angular drifts. The combined effect of these two causes was a more-or-less linear drift by amounts on the order of 10 nT/m during the 4.5 hours from start to finish of the data collection.

Without a thermal drift correction, the gradient tensor becomes increasingly inaccurate as a function of time with resultant striping parallel to the line direction and, in the high-density grid data, an obvious discontinuity between the data on either side of a 100-minute intermission in data acquisition. There is, however, no evidence that the thermal drift leads to significant common-mode leakage in the high-density data. Estimates show that the thermal drift would have to be an order of magnitude larger to cause noticeable common-mode leakage.

Removing Thermal Drift: The method for removing thermal drift from the high-density data takes advantage of the fact that, unlike field vector components, gradients are not very sensitive to small attitude variations. Therefore, a particular location was selected to serve as a thermal base station. Data were collected here at the beginning, middle, and end of the high-density survey. Because TESSA's attitude varied by only a few tenths of a degree in the reoccupations of the thermal base station, the gradients measured there should have remained nearly constant. Therefore, any change in those gradients was a measure of the thermal drift. As a result, the thermal drift was removed as two sets of nine linear functions defined between the nine gradients measured at the beginning, middle, and end occupations of the thermal base station location.

Magnetic-Field Curvature: As mentioned previously, TESSA was designed on the assumption that the gradient is effectively constant everywhere within the volume of a 1-m tetrahedron. But, this assumption cannot be applied to UXO work because of the target proximity. The gradient tensor only describes an infinitesimal point in space. Surrounding points conceivably can have differing magnetic fields and tensors subject only to the constraints that there be no discontinuities and that the equations governing magnetostatic fields are not violated. For purposes of discussion, this nonlinear potentiality is called field curvature.

The local magnetic field, within a volume of space (that is, TESSA) is fully described by an nth-order 3-dimensional vector polynomial that satisfies the magnetostatic laws, and the gradient tensor can be found easily by applying the gradient operator (∇) to each component of the vector polynomial. This is essentially taking the 1st derivative in a volume, resulting in a reduction of order by 1.

A Linear Field Polynomial: If the polynomial is order 1, the tensor will be order 0, which means that the field changes linearly as a function of location, and the tensor is everywhere the same; that is, each term of the tensor is a constant with respect to location. This system of equations can be solved completely with 8 vector field measurements (for example, three components at each of two sensors and two components at a 3d sensor). It is also the circumstance that TESSA was designed to handle because no field curvature is present.

In this case the system is slightly overdetermined because the TMGS, with the tetrahedral configuration, provides 12 simultaneous vector field measurements and, thus, a direct measure of all 9 tensor components. However, only eight field measurements are required because only five of the nine tensor components are independent. Therefore, because the system is overdetermined, the degree to which the nine-measured-component tensor departs from being symmetric and traceless becomes an indicator of the severity of the curvature.

Curvature of the Field Polynomial: If the field polynomial is order 2, then the tensor will no longer be constant. Each component now becomes a linear function of location because field curvature exists. In this case, 15 simultaneous field measurements are required and the tetrahedral configuration is slightly underdetermined. As the polynomial is increased to higher orders (n = 3, 4, …), the curvature deepens and it describes an increasingly more complicated magnetic field. It would be desirable to use vector field data in formulating a polynomial of sufficiently high order to describe the field of a nearby UXO target. Unfortunately, the TMGS does not provide enough simultaneous independent field-vector measurements.

Curvature of the Field from UXO Targets: Rudimentary modeling was performed to obtain a feel of scale for the curvature of nearby UXO targets. For a nearby (0.5 m) dipolar target it appears that, to obtain a sufficiently accurate tensor at the centroid of TESSA, the polynomial must be at least order 7 to 9. An order 7 polynomial has 80 degrees of freedom, meaning that 80 field-vector measurements are required for a solution; the TMGS has only 12. Therefore, the system is severely underdetermined and cannot begin to characterize, by simultaneous measurements of the 12 axes, the curvatures of nearby targets.

As a way out, one is tempted to think that 7 closely spaced TMGS readings (7 readings times 12 components per reading = 84 measurements) could be utilized in the polynomial solution. This cannot work, however, because the attitude of TESSA changes from reading to reading. Thus, common-mode leakage would dominate the solution, and the result would be correlated to ground-surface undulations instead of to the actual magnetic field.

There may yet be mathematical procedures for resolving the curvature issue by combining gradients (instead of field components) from several consecutive TMGS readings, but this level of modeling has not been performed. In the meantime, the high-density data were collected on a grid, allowing another option for resolving the curvature

problem, which will be discussed next. Nevertheless, the best solution is a future redesign of the sensor suspension apparatus to have smaller dimensions and a geometry that handles curvature more effectively while retaining the same number of sensors.

Minimizing the Effects of Curvature by Collocation of Gradients: With the tetrahedral configuration, the effective location of the measured gradient tensor is somewhere within the volume, nominally at the centroid, not in a direct line between any two sensors. However, the most accurate gradient measurements are those that lie on the baseline, and are assumed to be centered, between two sensors. The difficulty is that any single pair of sensors only provides three gradients when five are needed for the complete tensor. This means that the additional two gradients must be provided by another pair of sensors whose center is not in the same location as that of the first pair.

If field curvature is significant, the gradient from the second sensor pair simply belongs to a different tensor. The solution to the problem hinges on the fact that, unlike field vectors, the gradients are not very sensitive to small attitude variations. This means that, for constructing a complete tensor, individual gradients that are not yet part of a tensor can be shared among stations (fig. 4). Combining gradients from three different stations in this manner will reduce curvature effects as long as the attitude of TESSA does not change much from station to station—exactly the situation with the high-density grid, which was a nearly flat, horizontal surface.

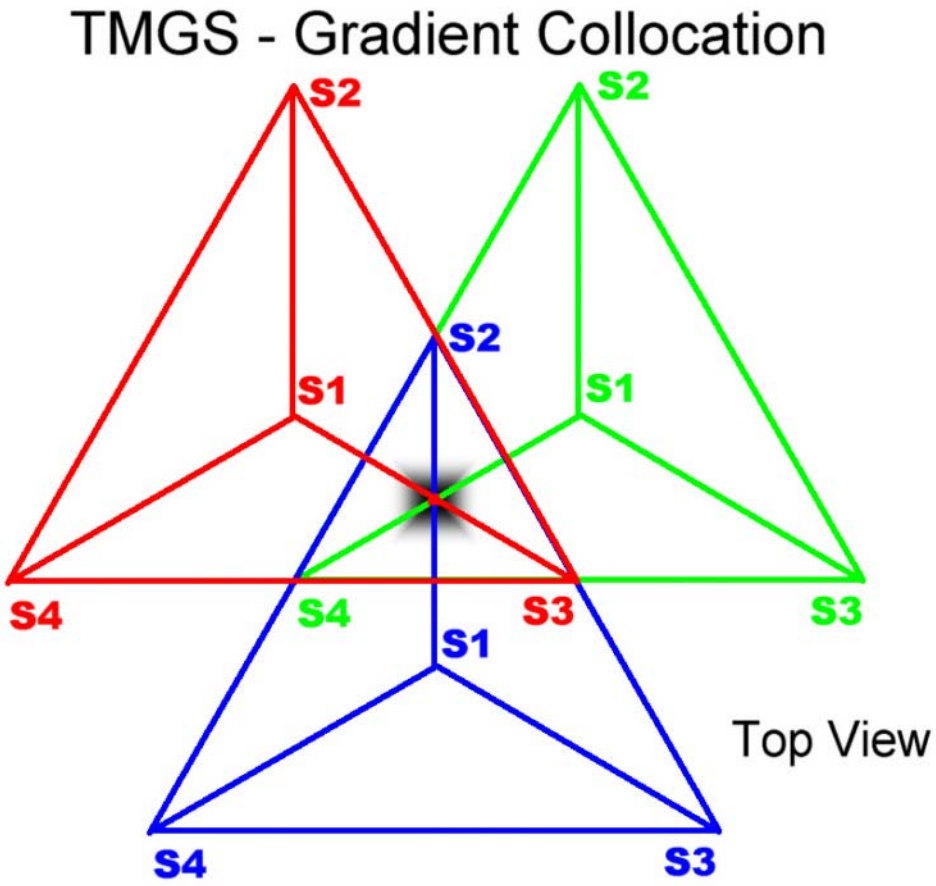

Figure 4. Gradients from three pairs of sensors (red s3-s1, green s4-s1, blue s2-s1) measured at three different stations (red, green, and blue tetrahedrons) are collocated at the point shown by a fuzzy black square to produce all nine components of a tensor.

Data Collection

Two different kinds of data were collected. The first kind was spatial data within the high-density grid. The second was angular data, derived from the spin calibration and used for deriving calibration coefficients applicable to all data collected at YPG during March 2003.

Spatial Data Collection in the High-Density Grid: The high-density grid is a 3-by-3-m horizontal area aligned on magnetic north and approximately centered on a known 60-mm UXO target, at 0.25-m depth. Also, eight additional known targets lie at regular intervals around the perimeter of the grid, four off the corners and four off the sides.

According to information supplied by YPG, consisting of independent testing of random soil samples and a separate magnetics survey conducted with a scalar gradiometer, there also appears to be significant magnetism randomly distributed within the soils, including clutter (fragments of exploded ordnance) within and outside the east half of the south side. The square grid cells are 0.25 m on a side, resulting in 13 rows and 13 columns of data-acquisition locations (169 stations), some of which were occupied more than once.

Stations were occupied beginning in the southwest corner, and proceeding north at 0.25-m intervals. After completing the northern-most station on a given line, TESSA was returned to the south end of the next line, 0.25 m farther east. Station locations were established by using a tape measure and spray-painting marks on the ground for alignment with calibrated marks on the cart. The resulting accuracy of the station locations should be plus/minus a few centimeters in both northing and easting. At each station, data were sampled at 0.2-second intervals for a minimum of 10 seconds (50 samples per station).

The data were collected in two stages, resulting in the two data files, n0312c and n0312d. The first stage went from line 1, point 1 (L1P1) through line 8, point 10 (L8P10). After a 100-minute hiatus, the second stage went from L8P10 through line 13, point 13 (L13P13), which is the final station in the northeast corner.

Spin Calibration: Data were collected for the express purpose of deriving precise coefficients used in reduction of TMGS data. The procedure is called spin calibration, in which TESSA is slowly rotated (within the Earth's large common-mode field) on a non-magnetic turntable. A complete circle plus 10 degrees of overlap was completed in just under an hour for each of four designated tetrahedron attitudes. The location for this procedure, different from that of the high-density grid, was chosen to minimize magnetic gradients. Temporal variations in the geomagnetic field were recorded by nearby scalar and vector base magnetometers. Spatial variations of the local magnetic field were obtained by performing a densely spaced survey using a scalar gradiometer.

The Coordinate Systems: The coordinate system for TESSA is Cartesian right-hand orthogonal with directions referenced to the positions of the magnetometer sensors. Refer to figure 1 and to one of the tetrahedrons shown in figure 4 to see how sensors s1, s2, s3, and s4 are arranged. The s1 sensor is at the top of the tetrahedron; s2, s3, and s4 form a horizontal triangle at the bottom of the tetrahedron. The x, y plane is parallel to the s2-s3-s4 triangle and runs through the centroid, which is vertically below s1 by exactly ¾ the tetrahedral height. The z-axis points down from the centroid toward the s2-s3-s4 triangle. (In figure 4, the z-axis points into the page from s1.) The y-axis is parallel to the line defined by s3-s4, with the positive sense toward s3. (In figure 4, the y-axis points to the right.) The x-axis is arranged in a right-hand system. (In figure 4, the x-axis points toward the top of the page.)

The origin of the high-density grid (geographic) coordinate system is at the grid point in the southwest corner at ground level. The positive z-axis points vertically down, the positive y-axis points magnetic east, and the positive x-axis points magnetic north.

TESSA was oriented on the high-density grid with its x-axis pointing magnetic north, y-axis east, and z-axis down—approximately co-oriented with the high-density grid coordinate system.

Processing Procedures

In this section, the data-processing procedures are explained, with particular objectives to elucidate each processing step according to the important concepts given previously and to illustrate how each processing step affects the gradient tensor. A flow diagram is given in figure 5.

Data Presentation: Considering that the gradient tensor itself is a complicated mathematical object that is not easily illustrated, other means of indicating data qualities must be sought. To this end, it should be noted that the data from the TMGS are comprehensive in the sense that they can be transformed into any of the four categories of magnetic field: scalar field, scalar gradient, vector field, or gradient tensor—the gradient tensor being the design objective and the most powerful of the categories.

The scalar field and scalar gradient can be easily illustrated in color-shaded relief. But having no particular sensitivity to field direction, neither of these can be a comprehensive indicator of the tensor qualities. The vector field includes the field directional information but, lacking a state-of-the-art attitude recovery system, it will be dominated by attitude-dependent noise. Also, having three components, it becomes difficult to illustrate. The remaining options are either (a) to prepare a large number of statistical devices that, while being quantitatively descriptive, rival the tensor's complexity, or (b) to find a qualitatively robust means of illustrating the tensor.

Determinant of the Tensor: Examination of the tensor reveals an assortment of qualities that may be utilized. In particular, each magnetic gradient tensor has an orthogonal natural coordinate system into which it can be rotated, called the principle axis frame. Performing the rotation diagonalizes the matrix; that is, all six of the gradient components that are not in the trace become zero. Also, the threeremaining components (g_{xx}, g_{yy}, g_{zz}) are a comprehensible set of gradients. (Only two of them are independent because $g_{zz}=-g_{xx}-g_{yy}$, which is required by Laplace's equation, $\nabla^2\Phi=0$).

If these three gradients are multiplied together, the result can be imagined to represent the volume of a box in gradient space—the bigger the box, the more gradient strength it contains. Furthermore, this object is a scalar quantity that can be easily illustrated in color-shaded relief as well as representing an intrinsic quality of the magnetic gradient tensor. Finally, this quantity is a tensor invariant (called the I_2 invariant) that can be

calculated easily from any reference frame by taking the *determinant* of the matrix—diagonalizing the matrix is not required (Pedersen and Rasmussen, 1990).

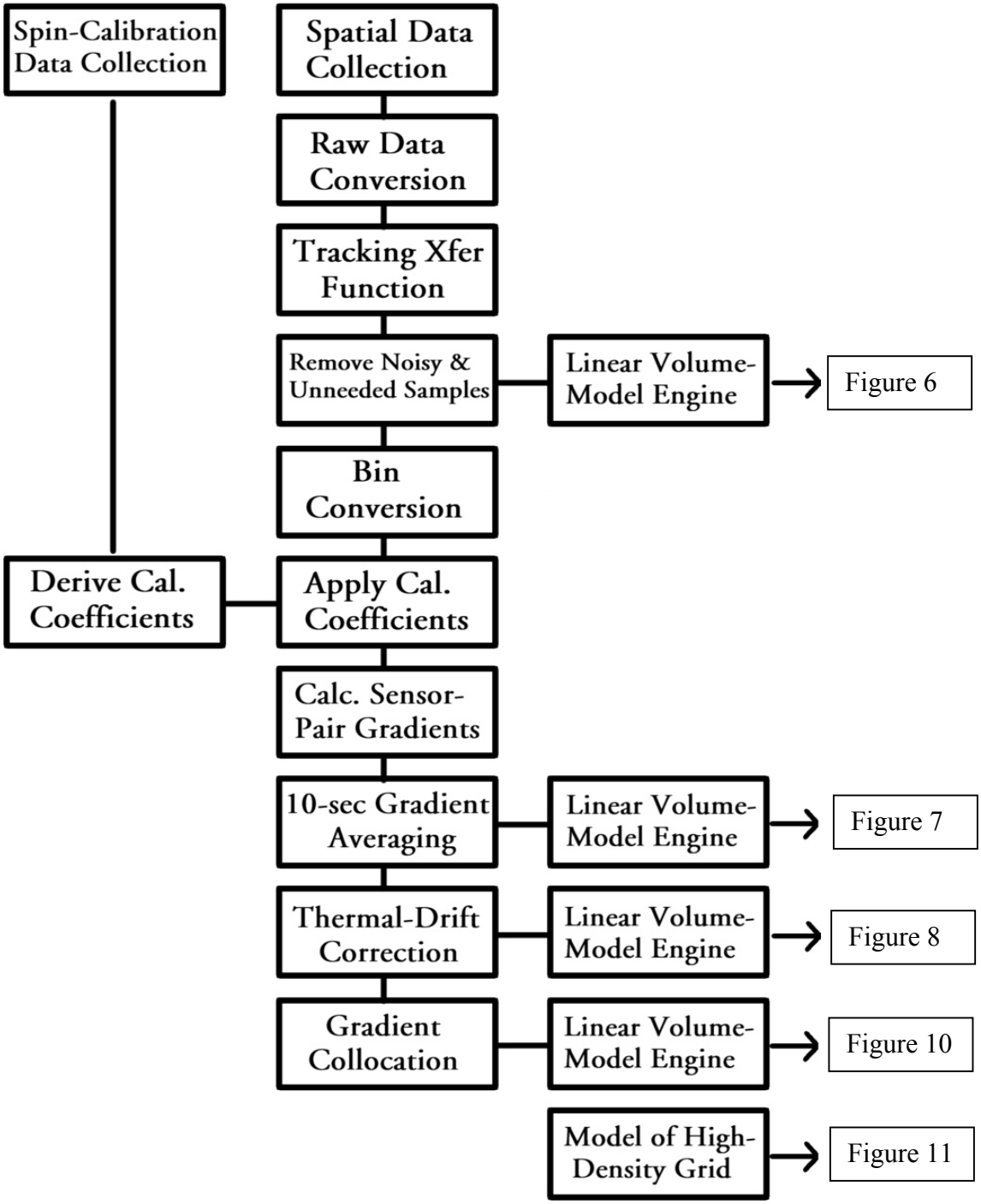

Figure 5. Flow diagram of data reduction showing the major processing stages for reduction to a tensor of the TMGS high-density data.

It can therefore be deduced that the magnitude of the determinant is in some way proportional to the proximity of a magnetic source. It actually goes by the 12th power of the inverse distance to the source. This results from the determinant being a product of three gradients, each of which follows an inverse 4th power law. The magnitude also has other characteristics dependent on the magnetic moments and the observation point. Evidently because of the influence of such an intense power law, the determinant has the greatest expression at the nearest approach to a source. In most cases, this means that a mapped determinant anomaly will reach a sharp (positive or negative) peak almost directly over its target. (Because of moment direction, the exact location of the peak may be offset slightly, or in some cases, the peak may be replaced with an abrupt positive-to-negative transition.) This is in contrast to a scalar-field anomaly that reaches an unfocused peak at a location somewhat offset from the target zenith.

Linear Volume-Model Engine: The linear volume-model engine is a utility computer algorithm that displays TMGS data, at various stages of processing, in a common format—namely the determinant of a gradient tensor. It allows data in a particular premature stage of processing to be examined in a mapped determinant form by converting them directly, without the intervening reductions. For example, figure 7 uses the engine to show what the mapped determinant would look like if the thermal-drift correction and collocation stages of data reduction were not performed.

The output is the determinant of the gradient tensor for each of the 169 stations in the high-density grid. The input, however, is allowed to be any of (a) raw TMGS data (analog voltages and bin numbers), (b) the 12 field-component values from the 4 TMGS sensors, or (c) the nine gradients obtained by subtracting the sensor readings (s2-s1, s3-s1, s4-s1). Therefore, the linear volume-model engine guarantees a standard nonbiasing procedure for TMGS data examination.

The linear volume model engine performs a two-stage process, the first of which converts the input data to 12-vector field components, and the second obtains a tensor (and its determinant) by applying a linear least-squares regression to the field components. Coefficients used in the first stage are nominal (for example, the magnetic sensor axes are assumed to be perfectly orthogonal). The regression in the second stage forces the trace to vanish by heavily weighting the trace summation equation, as suggested by Dr. Yaoguo Li, (Y. Li, oral commun., 2004). The regression, however, does not perform any other normalization. For example, weighting the least-squares system according to average field-component magnitudes introduces fictitious anisotropies; so, the engine does not perform this normalization.

Assumptions Applied to the Spatial Data: To simplify the processing of the high-density grid data, a number of assumptions were made about things that would not adversely affect the resulting tensor. These assumptions are the subheadings, as follows:

Positions match the ideal 0.25-m grid: The position recovery for both TESSA and the high-density grid is simply to use the planned values from positioning TESSA and setting

up the grid (for example, 1.25, 1.50, 1.75, … see "Spatial Data Collection in the High-Density Grid"). This means that there can be both systematic and random errors in the positions of TESSA amounting to plus/minus several centimeterss in x, y, and z.

Gradients vary too slowly as a function of attitude to warrant attitude corrections: The heading, pitch, and roll of TESSA changed by a few degrees each, from station to station. If the TMGS is not leaking common-mode field, this amount of change in attitude has only minimal effect on the gradients. Therefore, all gradients are assumed to have been measured in a common reference frame. However, it is important to mention that this is not a generally applicable assumption. In anything but the flattest terrain, attitude recovery must be performed for the gradients to within a couple of degrees in heading, pitch, and roll.

Sensor positions are coincident with the virtual tetrahedron vertices: As a foundation for tetrahedral calculations, an idealized tetrahedron with 97-cm edges is used and is called the virtual tetrahedron. Although they are fairly close, the true positions of the sensors do not exactly coincide with the vertices of the virtual tetrahedron. However, the errors are small, probably less than plus/minus 1 cm in each axis. This assumption would introduce less than a 1-percent error into gradient magnitude accuracies.

Sensor axes are coincident: By design, the three axes in each of the four magnetic sensors used in TESSA are not coincident; the x-, y-, and z-axes occupy different physical locations on each sensor base. This design presumes that readings are being taken in low-gradient regions (recall the original purpose of TESSA), contrary to the UXO detection circumstance. Similarly, it violates one of the prerequisites mentioned earlier for obtaining the three components of the magnetic field vector; namely, that the axes must be coincident.

However, the designing of a data-reduction procedure to correct this inadequacy was not performed. Indeed, such a procedure would have improved the results but was not critical in meeting the objectives of this study. Therefore, assuming the axes on each sensor to be coincident has introduced up to a plus-or-minus 4-percent error into the gradients. This has the potential to reduce the determinant accuracy by as much as plus-or-minus 12 percent, a fairly large amount. However, a future design of the sensor suspension apparatus can minimize or obviate the need for a sensor-axis coincidence correction by taking advantage of the fact that the three axes on each sensor are collinear.

Assumptions Applied to the Spin-Calibration Data: To simplify the processing of the spin-calibration data, a number of assumptions were made about things that should have minimal effect on the resulting tensor or could be reduced by other means. These assumptions are the italicized subheadings, as follows:

The background field was stable and its tensor everywhere zero: For derivation of all the spin calibration coefficients, it was assumed that the geomagnetic field did not vary as a function of time. Also, it was assumed that the magnetic gradient tensor was zero

everywhere within the volume of space required for the spin calibration. Though neither of these assumptions is strictly valid, measurements of both the temporal and spatial scalar field during the calibration showed that the variations would not significantly affect the coefficient values. Therefore, the spin-calibration data were reduced using the assumption that the scalar field was a temporal and spatial constant of 48,000 nT. However, the necessary temporal and spatial data were collected, so if it later becomes apparent that improved accuracy of the coefficients is necessary, these data can be applied.

Sensor 1 is perfectly aligned with the virtual tetrahedron: Sensor 1 (s1) was used as a reference for converging the attitudes of the other sensors (s2, s3, s4) so that all four sensors can be mathematically rotated into a common coordinate system. However, no attempt was made to ascertain the attitude of s1 relative to the virtual tetrahedron. Therefore, it is quite likely that s1 is misaligned with the tetrahedron by a degree or so in heading, pitch, or roll. As a consequence in the final tensor, the field directions and the gradient baseline directions are slightly misaligned, which has only a very small effect on the tensor values.

The sensor temperatures did not vary: Many of the coefficients derived from the spin-calibration data are functions of temperature. However, the deeply involved data-acquisition procedures that were required to define these functions were not performed. Consequently, the coefficients were derived as if the temperatures were constant (although the temperatures were measured), and reliance was placed upon the thermal-drift correction to supplement the missing data.

Raw-Data Conversion: The first processing stage is to convert from the data file recorded in the field to an in-house format for manipulation in postprocessing.

Basic Data Forms: The raw data are recorded as an analog voltage that converts to magnetic field at the approximate rate of 100 nT/V. To maintain core linearity and signal precision, the magnetic flux through the core is minimized by applying an opposing magnetic field (a bucking field), which is incremented every few hundred nanoTeslas of field change. The amplitude of the bucking field is recorded as an integer value ranging from –256 to +255 and is called the bin, or bin number. The analog voltages and bin numbers from all 12 axes of the 4 magnetometers are recorded simultaneously every 0.2 second with 16-bit precision to maintain tracking and 0.02-nT precision levels. In the high-density data, 1-Hz analog anti-alias (low-pass) filters were used before sampling. Auxiliary data streams also were recorded at the same rate for sensor temperatures, Morris temperature (temperature inside Morris), air temperature, and tilt (pitch and roll).

Recording Method: All channels were recorded continuously for each data file with documentation fiducials (doc points) marking the beginning and end of each station collection period. The recording program, called KMGR7, is coded in C++ and produces several ASCII subfiles with hexadecimal values. Two subfiles will fit on a 1.38-Mb diskette.

Conversion Program: The subfiles are interpreted, concatenated, and converted to an in-house file format for further processing. In this file, analog voltages and bins are unmodified and are preserved as exactly the values that were recorded. Doc points and associated data-acquisition operator comments are separated into separate files for independent viewing and input to subsequent programs.

Deconvolving Bin Steps from Analog, and Matching Axes for Precision Tracking: The TMGS can be understood as a linear system that responds as a function of frequency. Yet, the calibrations that are performed are effectively done at D.C. (wave number 0). This means that not all the calibrations hold for the low-frequency signals that would be expected during data acquisition from a moving platform. Consequently, it is necessary to establish a transfer function for each axis of each magnetometer that effectively ties the amplitudes and phases in the Nyquist interval back to the measured D.C. levels. This ensures that the 12 axes will track together up to a prescribed precision, and that step functions (injected into the analog voltage whenever a bin changes) can be handled without introducing significant discontinuities in the axis signals (see below, "Bin Conversions").

The transfer functions have been measured over the current Nyquist interval (0 to 2.5 Hz) and found to be quite stable. However, they have not been applied to the high-density data because the data were effectively collected at wave number 0.

Removal of Intervening Data Records and Noisy Samples: Using the doc points, all records that were not acquired during the 10-second station-sampling period are removed. Any records contaminated with obvious spiking or other noise processes are also deleted. The x and y positions in the high-density grid coordinate system are added to the file at this time. Figure 6 illustrates the determinant that would result if the data were left in its raw form, without any further processing.

Bin Conversions: For each of the 12 axes, the bin numbers are converted to equivalent voltages at a nominal rate of 5 V/bin for s1 and s2, and 3.3 V/bin for s3 and s4. (The differing conversion rates reflect two slightly different manufacturers' model lines.) The equivalent voltages are then combined with the corresponding analog voltages to produce 12 axis signals that can range from –800 to +800 V. (This voltage range, combined with the nominal 100 nT/V signal-to-field conversion, implies a –80,000-nT to +80,000-nT field range.) In general, the exact voltage associated with each bin number must be ascertained in the laboratory and is a complicated function of bin number, sensor temperature, and Morris temperature. However, rather than a direct measure of the bin number-to-voltage conversion, a more precise quantity is measured, called the bin-step size. It is simply the amount of voltage change associated with a step from a given bin to one of its neighboring bins.

Although a comprehensive discussion of the dependencies between the bin conversion functions and the axis polynomial (described in the next section) is well beyond the scope of this writing, it suffices to say that accurate knowledge of each bin-step size reduces common-mode leakage, minimizes bin-step discontinuities, and improves tracking when taking measurements from a moving platform. An inaccurate knowledge of the bin-step size will introduce noise that manifests as a sawtooth of pseudo-random amplitude and wavelength riding on a changing field (typically, the Earth's common-mode field).

While the laboratory bin-size calibrations have not yet been completed, it is expected that the bin-step sizes can be known to about 0.05 nT. Until then, preliminary bin voltage conversions have been used, with apparent bin-step size errors on the order of 1 nT. It should be noted that, in the high-density data, bins were fairly constant with occasional changes of plus/minus 1 bin step. Table 1 lists bin-step sizes used in reducing the high-density grid data.

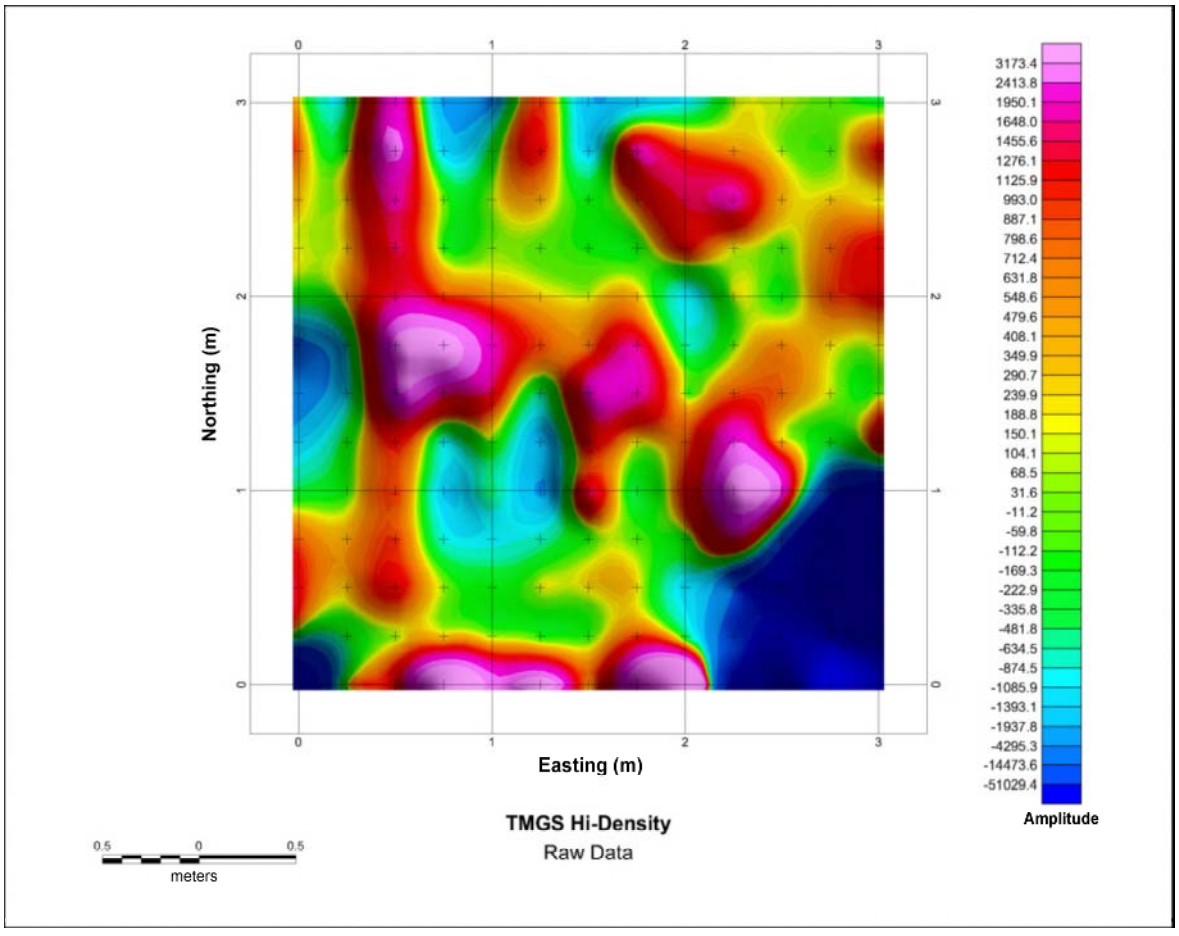

Figure 6. Raw TMGS high-density data processed by the linear volume-model to a determinant of the magnetic gradient tensor. The map is correlated primarily to ground surface undulations due to common-mode leakage of the Earth's primary field, resulting from application of nominal calibration coefficient values. The color scale is nonlinear.

Table 1. Average bin sizes <volts/bin>.

Axis	Sensor 1	Sensor 2	Sensor 3	Sensor 4
x	5.046971	5.050641	3.302770	3.308334
y	5.048011	5.054041	3.311700	3.307056
z	5.044710	5.056564	3.304325	3.312998

Application of Spin-Calibration Results for Converting Voltages to Fields: The spin calibration procedure essentially nulls the Earth's common-mode field as a function of attitude by slowly spinning TESSA and then applying a nonlinear regression to the resulting data. The coefficients derived through the spin calibration are applied to the high-density grid axis signals (resulting from bin conversions) to calibrate and align the sensors.

The proper application of the spin-calibration coefficients is critical to a successful data reduction. Because some of the associated derivations are also tedious, a Fortran subroutine called s_ab2h.f is provided in Appendix A to clarify how the spin calibration data are used. This subroutine applies the bin-size, axis polynomial, orthogonality, and sensor attitude coefficients to basic TMGS analog and bin data. A mathematical derivation of the spin-calibration procedure is provided in Bracken and others (2005).

Axis Polynomial: The axis polynomial is a third-order fit of the axis signal to its corresponding magnetic field component. For each axis, it effectively calibrates the zero-offset, and the gain, which are respectively the 0th- and 1st- order terms of the polynomial. The axis polynomial and the orthogonality correction are solved simultaneously for all three axes on a given sensor by requiring that the scalar field be correct for all attitudes. Tables 2, 3, 4, and 5 list the coefficients of the axis polynomial. The zero-offset is the magnetic field present when the axis signal is 0. The gain is the rate of change in magnetic field with respect to the axis signal voltage. The quadratic and cubic terms are only a small contribution, indicating that the magnetometer response is extremely linear. (In each table, the least significant digit displayed is consistent with a 0.01-nT precision level.)

Table 2. Axis polynomial – constant term (zero-offset) <nanoTesla>.

Axis	Sensor 1	Sensor 2	Sensor 3	Sensor 4
x	–51.57	–34.78	5.84	20.28
y	–50.33	12.95	7.4	35.23
z	–56.54	–18.86	–25.86	5.18

Table 3. Axis polynomial – linear term (gain) <nanoTesla/volt>.

Axis	Sensor 1	Sensor 2	Sensor 3	Sensor 4
X	99.95753	99.04721	99.36614	99.80745
Y	101.12474	100.75199	100.41647	100.63311
Z	99.06592	99.43129	99.76678	99.13475

Table 4. Axis polynomial – quadratic term <nanoTesla/volt^2>.

Axis	Sensor 1	Sensor 2	Sensor 3	Sensor 4
X	–0.00001834	–0.00000565	0.00001941	0.00000958
Y	–0.00002865	0.00000174	–0.00001841	–0.00003666
Z	0.00018719	0.00007021	0.00004180	–0.00009373

Table 5. Axis polynomial – cubic term <nanoTesla/volt^3>.

Axis	Sensor 1	Sensor 2	Sensor 3	Sensor 4
X	0.00000000514	–0.00000007088	0.00000000596	–0.00000013659
Y	0.00000002123	0.00000000462	–0.00000000101	–0.00000016287
Z	0.00000041569	0.00000007837	–0.00000007556	–0.00000029001

Orthogonality Correction: The three axes of a given magnetometer are not quite perpendicular. Therefore, the orthogonality correction mathematically realigns them into a nearly perfectly orthogonal rectilinear coordinate system. Table 6 gives the actual angles between the three axes on each of the four sensors.

Table 6. Orthogonality correction angles <degrees> (x is fixed in space; y "moves" only in the x-y plane).

Axis	Sensor 1	Sensor 2	Sensor 3	Sensor 4
y-x	89.89108	90.11640	89.82039	90.24590
z-y	90.75768	90.01508	91.26369	89.72196
z-x	89.72650	89.56956	90.21198	89.10476

Attitude Correction: The attitude correction is performed as a separate regression from the axis polynomial and orthogonality, but uses the same spin-calibration data sets. It aligns sensors s2, s3, and s4 with sensor s1 (see previous section "Assumptions Applied to the Spin-Calibration Data"). In other words, it mathematically rotates all four sensors into a common reference frame, the coordinate system for TESSA. Table 7 shows the ideal, and table 8 shows the measured attitude correction angles derived from the spin-calibration data.

Table 7. Ideal attitude angles <degrees>. (Positive is CW rotation about axis as viewed from sensor origin).

Axis	Sensor 1	Sensor 2	Sensor 3	Sensor 4
z'''	0.00000	0.00000	120.00000	–120.00000
y''	0.00000	–109.47122	–109.47122	–109.47122
z'	0.00000	180.00000	60.00000	–60.00000

Table 8. Actual measured attitude angles <degrees>. (Positive is CW rotation about axis as viewed from sensor origin).

Axis	Sensor 1	Sensor 2	Sensor 3	Sensor 4
z'''	0 assumed	–0.43250	121.59830	–119.26004
y''	0 assumed	–109.35126	–110.02656	–109.88480
z'	0 assumed	180.12615	60.42545	–59.63062

Temperature Corrections: The coefficients in the axis polynomial are functions of sensor temperature rather than simple constants. Similarly, the angles used in the attitude correction are functions of outside temperature, actually the temperature of TESSA. However, these coefficients were measured as constants rather than functions of temperature. As a result, the gradients from the high-density grid had to be corrected for thermal drift as is described in the section “Thermal-Drift Correction.”

Differencing Magnetic Fields to Obtain Initial Gradients: From this point, subsequent reductions must be performed on gradients. Therefore, three gradient baseline directions are found for each 0.2-second sample. (There are six baselines, but only three form a basis for a coordinate system because the remaining three are linearly dependent upon the first three.) Because of reductions already performed (simultaneous sampling, transfer-function matching, proper bin conversions, and spin calibration), these gradients are sealed against a variety of common-mode leakage problems, including the Earth's common-mode field.

The gradients are then found by subtracting the three field components of sensor s1 from each of the three remaining sensors, s2, s3, and s4, and then dividing by the sensor separation distance of 0.97 m. The gradient baseline directions in the TESSA coordinate system are listed as follows in table 9.

Table 9. Azimuths and dip in degrees of the three sensor-pair gradient baselines. The coordinate system is geographic with TESSA level and pointing magnetic north (azimuth 0 deg). For clarity, the specific gradients associated with each of the three sensor pairs are shown as well.

Sensor pair	Azimuth	Dip	Gradients
S2-s1	0°	54.7°	$\partial b_x/\partial 21$, $\partial b_y/\partial 21$, $\partial b_z/\partial 21$
S3-s1	120°	54.7°	$\partial b_x/\partial 31$, $\partial b_y/\partial 31$, $\partial b_z/\partial 31$
S4-s1	240°	54.7°	$\partial b_x/\partial 41$, $\partial b_y/\partial 41$, $\partial b_z/\partial 41$

Obviously, these gradient baselines have not been rotated into an orthogonal coordinate system, as have been the field components. Because subsequent processing steps need only work on individual gradients, however, this rotation need not be done. Also, where the field components were extremely sensitive to the attitude of TESSA, these gradients change very slowly with attitude and are therefore much more easily handled.

Ten-Second Averaging of Gradients to Obtain Station Gradient Data: For each station in the high-density grid, each of the nine gradients calculated in the previous step was averaged over a 10-second period (50 samples at 0.2 second per sample). Assuming that the noise is Gaussian, averaging 50 samples increases the precision and confidence of the station by a factor of 7 over that of any single sample, using the $\sqrt{n}$ rule. In theory, this averaging step can only be performed on the gradients, not on the field components, because the combining of field components in any manner before spatial differentiation breaks the seal and allows common-mode leakage to reenter the system. In practice, with the high-density data, had the averaging been done before the gradients were calculated (which it was not), the error would have been almost insignificant. Figure 7 illustrates the determinate that would result if the data were processed only up through 10-second averaging.

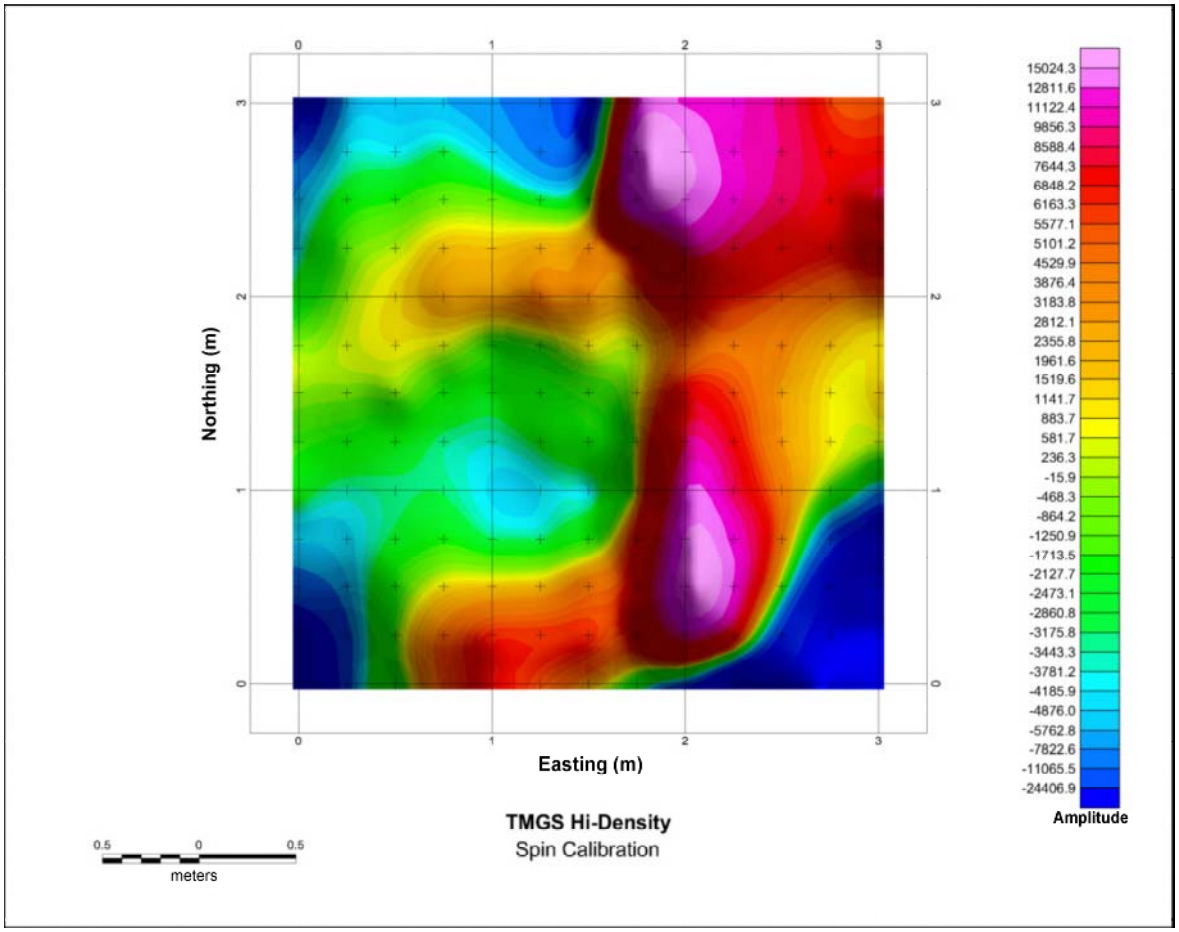

Figure 7. Calibrated TMGS high-density data processed by the linear volume-model to a determinant of the magnetic gradient tensor. Application of the calibration coefficients (from the spin calibration) to the field components, and subsequently finding the gradients by differencing the field components in each sample, removed the common-mode leakage, leaving thermal drift as the dominant of the remaining nongradient effects. Therefore, this map is correlated primarily to thermal drift while the ground-surface undulation effects of the previous figure have been removed. It is instructive to observe that the major feature on this map coincides with the 100-minute hiatus between data sets, during which time the temperatures of the sensors continued to climb.

Thermal-Drift Correction: Thermal drift was removed from the gradients, as described previously. The thermal base station, in the southwest corner of the high-density grid, was used as the reference location and was occupied three times during data collection: at the beginning, in the middle, and at the end. Each of the nine gradients described previously ($\partial b_x/\partial 21$, $\partial b_y/\partial 21$, $\partial b_z/\partial 21$, $\partial b_x/\partial 31$, and so forth) was treated independently of the others in setting up a thermal baseline for each of the two data files (n0312c and n0312d).

The baselines required that each gradient at the thermal base station remain constant over the duration of the data collection, and the resulting correction was applied as a linear function of sensor temperature to the intervening stations. The thermal drift rates ranged from 0 to 2.6 nT/m per degree Celsius (sensor temperature) depending on which gradient was being considered. The sensor head temperatures increased at about 2.3 degrees Celsius per hour over the 4.5-hour duration of the combined data sets.

Unknown Constant: Because there was an unknown amount of thermal drift between the high-density and the spin-calibration data collections, the true value of each gradient at the thermal base station had to be considered an unknown constant value. The constant was estimated for each of the nine gradients by subtracting the gradient's average (over the entire high-density grid) from its thermal base station value after removal of the thermal drift. In other words, each of the nine gradients was adjusted by removing its average value.

In Lieu of Temperature-Dependent Spin-Calibration Coefficients: Had the coefficients derived from the spin-calibration data contained the appropriate thermal dependencies, this entire thermal drift correction would have been obviated. Although it is anticipated that future TMGS data reductions will use thermally dependent coefficients, good field practice predicates that provisions for thermal corrections always be made. That is, a base location should be reoccupied every few hours of data collection. Figure 8 illustrates the determinant that would result if the data were processed up through the thermal drift correction.

Gradient Collocation: Because of field curvature, each of the nine sensor-pair gradients ($\partial b_x/\partial 21$, $\partial b_y/\partial 21$, $\partial b_z/\partial 21$, $\partial b_x/\partial 31$, and so forth) is potentially in a different location than any of the others. Due to the mean value theorem (a basic theorem of calculus), a gradient calculated by differencing does exist on the line segment between the two bounding sensors, but its exact location is not known (fig. 9). (The collocation procedure described here cannot mitigate this effect of curvature between sensor pairs, but it can move the sensor pairs into the same volume of space.) If the gradient-producing system is random, however, the most probable gradient location is halfway between the sensors. This is the assumption that must be made unless future modeling shows that the probable gradient location is skewed due to sources always being below TESSA. Therefore, the most probable gradient locations (halfway between sensors) are given as follows, in table 10.

Table 10. Expected x, y, and z coordinates in meters of the locations that are halfway between sensors. The origin is at the centroid in the TESSA coordinate system. The specific gradients associated with each of the three sensor pairs are included.

Sensor pair	X (m)	Y (m)	Z (m)	Gradients
s2-s1	0.280	0.000	-0.198	$\partial b_x/\partial 21$, $\partial b_y/\partial 21$, $\partial b_z/\partial 21$
s3-s1	-0.140	0.243	-0.198	$\partial b_x/\partial 31$, $\partial b_y/\partial 31$, $\partial b_z/\partial 31$
s4-s1	-0.140	-0.243	-0.198	$\partial b_x/\partial 41$, $\partial b_y/\partial 41$, $\partial b_z/\partial 41$

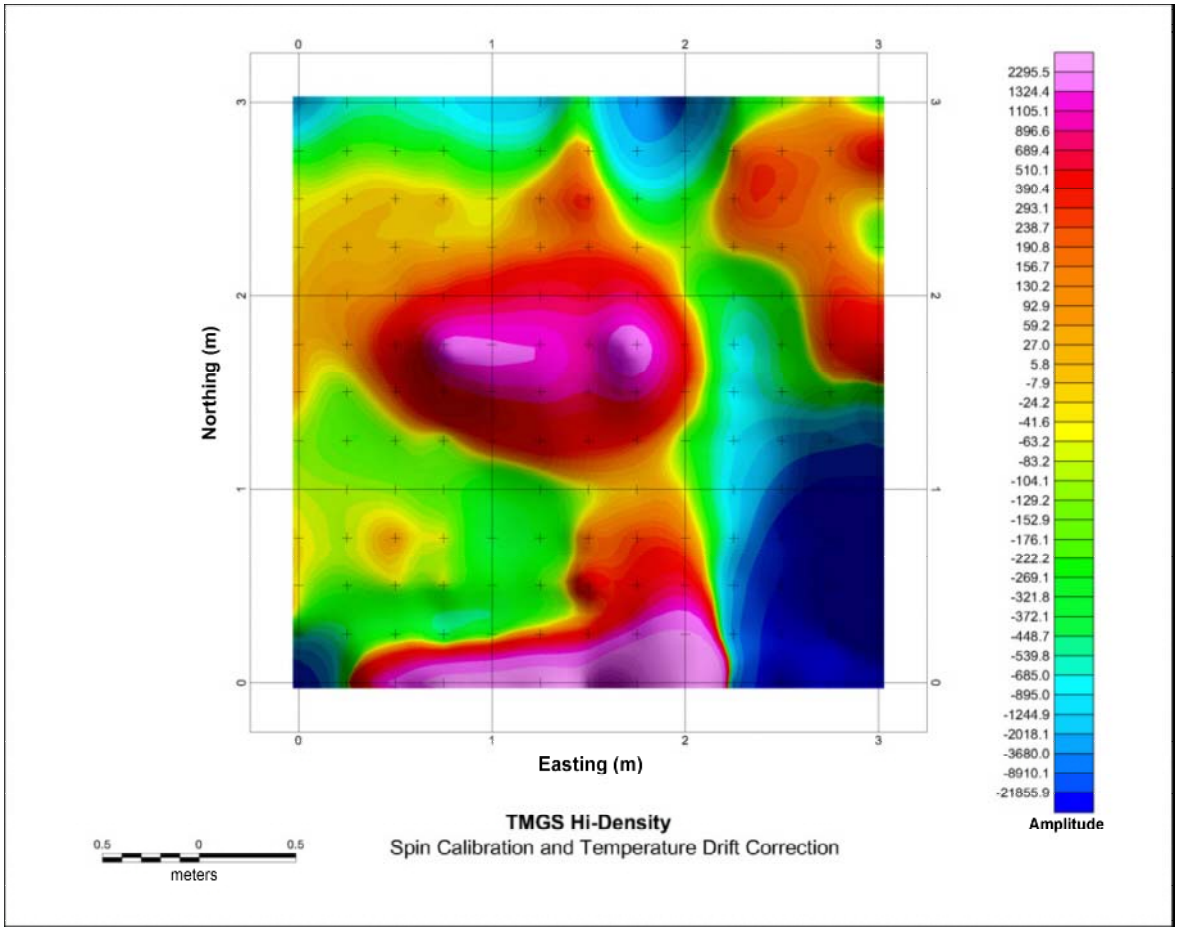

Figure 8. Thermal-drift corrected TMGS high-density data processed by the linear volume-model to a determinant of the magnetic gradient tensor. With the dominating effect of thermal drift removed, the true anomalies have become visible. Yet, they are distorted and unfocused due to the remaining nongradient effects of field curvature.

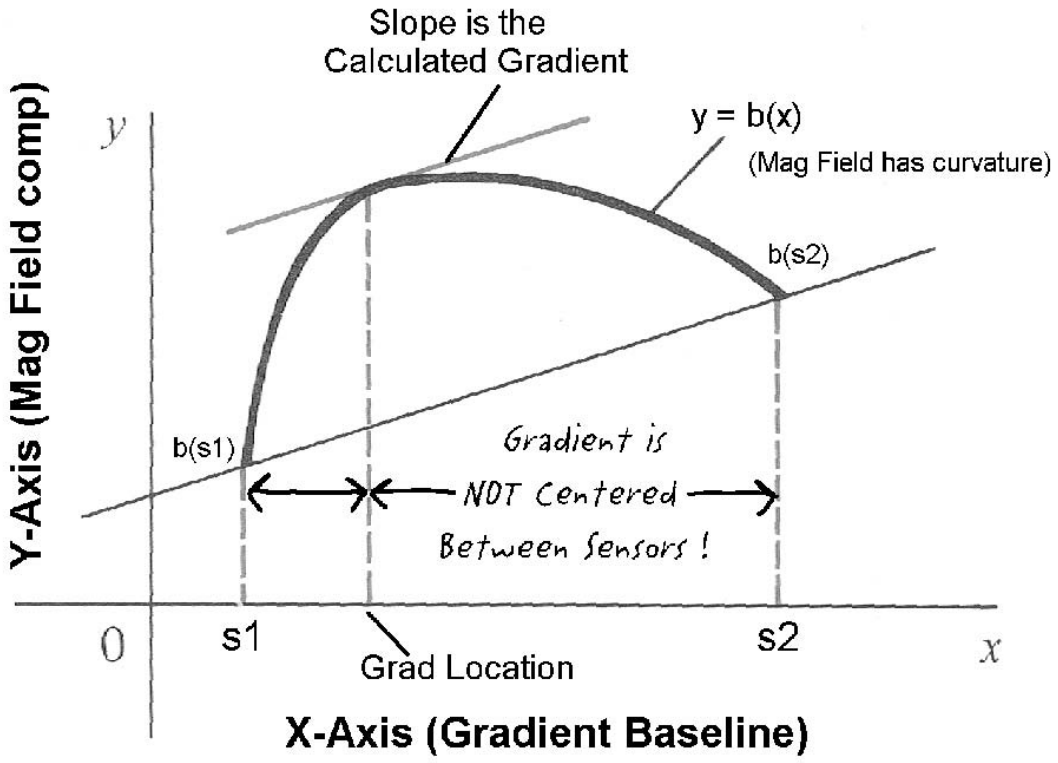

Figure 9. Illustrates the implications of mean value theorem, that (a) if a gradient is calculated by taking the difference of field components from two sensors, then the gradient exists and it lies somewhere between the two sensors; and (b) the location of the calculated gradient is not constrained to be at any particular place between the two sensors.

Apparently, the set of three gradients calculated from any pair of sensors is nearly 0.5 m from the gradients of either of the other two sensor pairs. Considering that the entire anomaly is scarcely more than 1 m in diameter, it is not difficult to see that these gradient pairs must be mathematically collocated before they can be combined into a coherent tensor.

To implement the methodology described previously ("Minimizing the Effects of Curvature by Collocation of Gradients," and figure 4), each of the nine gradients was treated individually as a scalar function of x-y position. Initially, the positions used were the centroid's x and y, which are the same as the station locations. Each of the 13 north-south data-collection lines was smoothly (1-d) interpolated to a 1-cm interval, preserving gradient values, and all derivatives. Then at a given station location, each gradient was replaced with an appropriately offset value from the same line or from an adjacent line.

For example, to accumulate the collocated gradients at station L7P7 (line 7 point 7, in the exact center of the high-density grid), the s2-s1 gradients were replaced with values from the same line interpolated at 28 cm south. This location is near L7P6, which is 25 cm to the south. In fact, the actual location of the s2-s1 gradients from station L7P6 is about 3 cm north of station L7P7.

The s3-s1 gradients were replaced with values from line 6 interpolated at 14 cm north. This location is just over halfway between L6P7 and L6P8. The actual location of the s3-s1 gradients from station L6P8 is about 11 cm north and 0.75 cm west of L7P7.

The s4-s1 gradients were replaced with values from line 8 interpolated at 14 cm north. This location is just over halfway between L8P7 and L8P8. The actual location of the s4-s1 gradients from station L8P8 is about 11 cm north and 0.75 cm east of L7P7.

Therefore, if it can be assumed that the gradient values are located halfway between sensors, the collocation algorithm actually implemented is fairly precise in the north-south direction, but it smears the gradients over a 1.5-cm-wide east-west zone. Nevertheless, this is an acceptably small error.

Finally, extrapolation was performed around the edges of the high-density grid to supply missing information for bordering rows and columns. This may have reduced the tensor accuracies on lines 1 and 13, and on points 1, 2, and 13 of all lines, covering nearly 40 percent of the high-density grid area around the edges. This means that any statistical chart of the collocated high-density grid data will be skewed unless these rows and columns are first eliminated from the statistical analysis.

Converting Sensor-Pair Gradients to a Tensor: At this point in the processing of the high-density grid data, the gradients (s2-s1, s3-s1, s4-s1) are ready for conversion to a tensor. Because all nine gradients have been measured and only five are required, the tensor is slightly overdetermined. At least two ways exist for computing the tensor.

By Rotation: Although this method is not described in detail here, the most obvious way of computing the tensor is to rotate the gradients first into an orthogonal coordinate system and then rotate that into the coordinate system of TESSA, in order to coincide with the coordinate system of the field components. Both of these rotations can be done simultaneously by standard matrix multiplication between the matrix of column vectors ($\partial b_i/\partial 21$ $\partial b_i/\partial 31$ $\partial b_i/\partial 41$) and an appropriately derived rotation matrix. It should be noted that rotating a finalized tensor requires a similarity transform to rotate both the field components and the gradient baseline directions; but here, only the baseline directions need to be rotated.

The rotation approach yields a nine-component tensor that is asymmetric and has a non-vanishing trace to the extent that there was residual curvature or other noise in the measurement and reduction processes. It has the potential to be a good diagnostic tool except that the rotation tends to mix up noise from the various sensor-pair gradients.

Nevertheless, the determinant of the tensor derived in this manner is still fairly representative of the system capabilities.

By Linear Least Squares Regression: Another method of converting the (s2-s1, s3-s1, s4-s1) gradients into a tensor is by backing out relative field components at the sensors and then applying to them a linear least-squares regression, as is done by the Linear Volume-Model Engine (previously described). Therefore, the Linear Volume-Model Engine is used here to calculate the final tensor and determinant from the collocated (s2-s1, s3-s1, s4-s1) gradients. This is illustrated in figure 10 with corroborative modeling shown in figure 11.

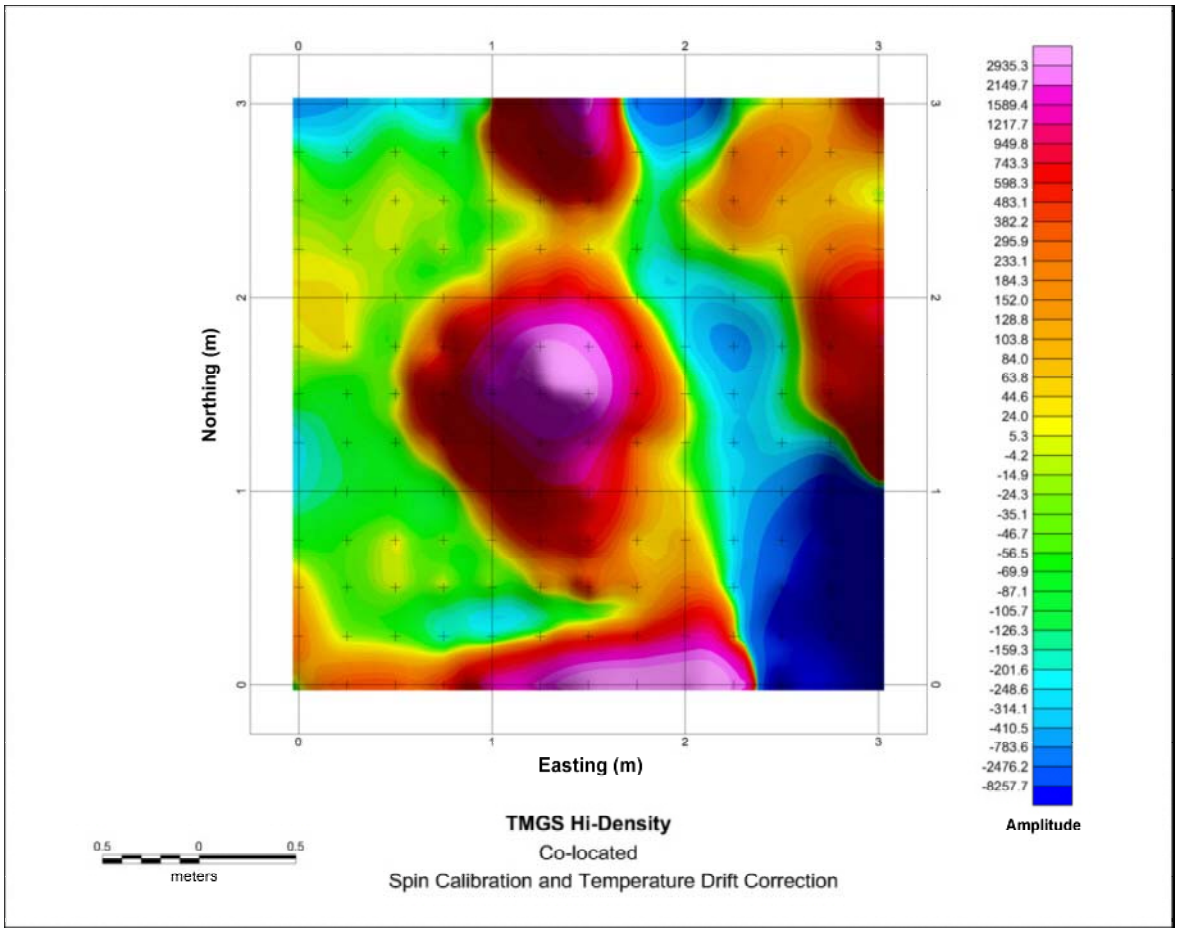

Figure 10. Collocated TMGS high-density data processed by the linear volume-model to a determinant of the magnetic gradient tensor. Collocation of the gradients measured by TESSA has largely mitigated the distortions caused by field curvature. This result approaches the map produced by modeling fields from the targets.

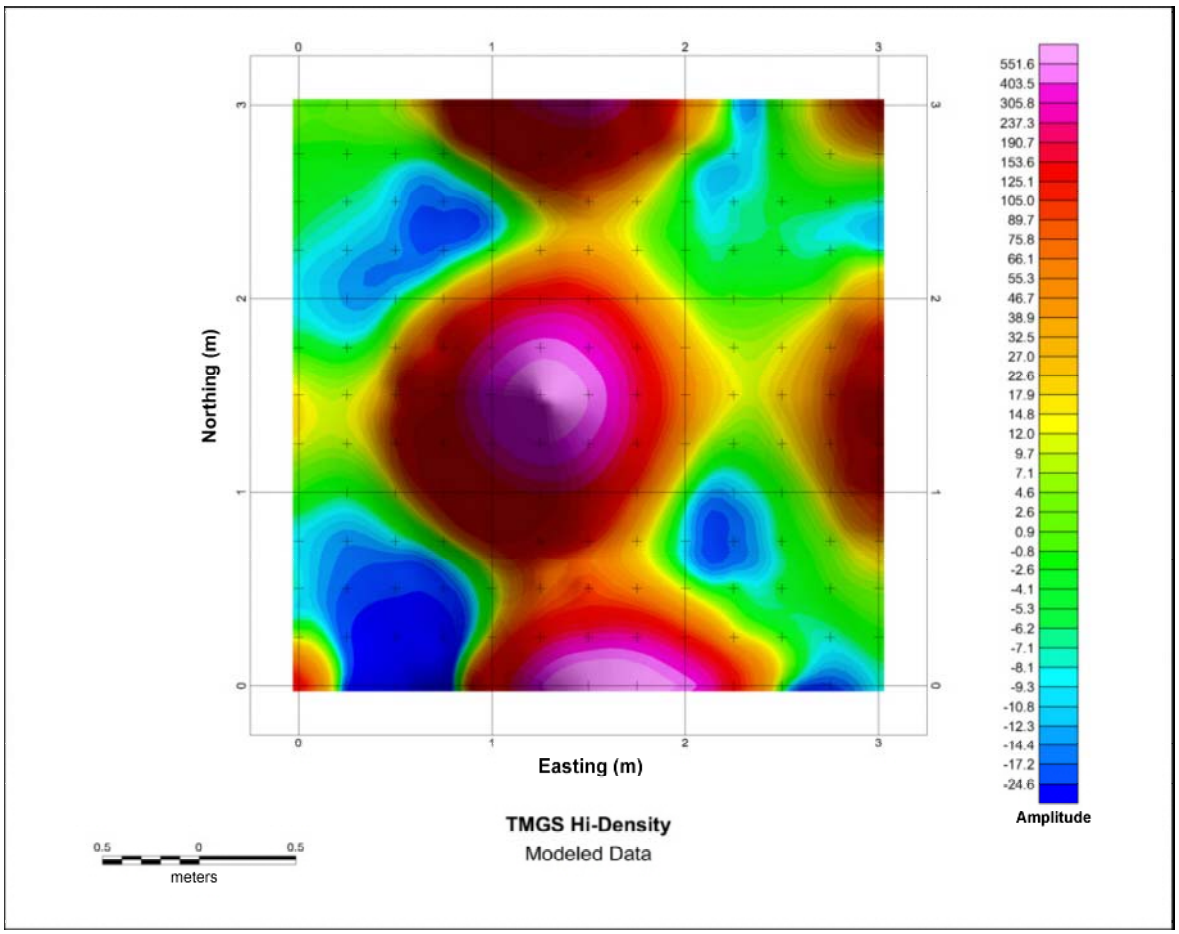

Figure 11. Model of the high-density grid targets, processed to a determinant of the magnetic gradient tensor. The magnetic fields of the center target, a 60 mm UXO at 0.25-m depth, and the eight edge-targets were modeled by assuming the depth and approximate location specifications provided with the Calibration Grid. Horizontal positions were adjusted slightly to account for positioning inaccuracies of both the target and TESSA. Magnetic dipole moment directions were assumed to be in alignment with the Earth's field (preliminary modeling shows this assumption to be somewhat in error, but use of the modeled directions would become circular reasoning in this application); but moment magnitudes were adjusted to match anomaly peaks. This figure is preliminary, intended only for qualitative comparisons with figures 6, 7, 8, and 10. A more precise model is described in the next section and shown in figure 13, which is for comparison with figure 12.

A Model of the Expected Tensor Determinant

To illustrate the capabilities of the TMGS, a model was produced of the expected fields from the nine UXOs that were buried in and around the high-density grid. Because this

model was not rigorously derived, using it for in-depth quantitative analyses is not recommended. However, it does demonstrate conclusively that the TMGS, in its current form, produces a realistic tensor with a better than expected detection capability.

A forward modeling routine was used that calculates the magnetic field, the magnetic gradient tensor, and the determinant of the tensor generated by any given spatial arrangement of point-dipole sources. The location and dipole moment of each source must be specified. An object of any shape can be modeled by specifying a sufficient quantity of point sources within its boundaries. Here, only one source was used for each of the nine UXO, assuming the targets to be sufficiently represented by a single point dipole. No attempt was made to model anomalies caused by clutter and geologic sources.

Parameters of the forward model are:

- The height of the measurement surface in negative meters above the ground surface;
- the x, y location of the observation point;
- the magnitude, declination, and inclination of the Earth's magnetic field;
- the depth in positive meters below the ground surface of the dipole being modeled;
- the dipole's x, y location; and
- the dipole's moment magnitude, declination, and inclination.

The height of the measurement surface was fixed at –0.88 m, corresponding to the height of the most probable gradient measurement locations (see the z coordinate in table 10). The depth of each dipole was fixed at the known depth of its corresponding UXO target obtained from the "ground truth" information supplied for the YPG calibration grid (table 11).

Table 11. Values used for the dipole modeling of the UXO targets. The UXO ID corresponds to the numbers listed on the target locations in figures 12 and 13. The X-Location and Y-Location model parameters were adjusted within a 0.25-m boundary of expected positional error. The Dipole Moment magnitude was adjusted to match modeled anomaly amplitudes to measured amplitudes.

UXO ID	X Location (meters)	Y Location (meters)	UXO Type	UXO Depth (meters)	Dipole moment (Ampere-Meter×Meter)
1	–0.30	–0.30	M75	0.15	0.0500
2	1.60	–0.40	60 mm w/ clutter	0.25	0.1380
3	3.40	–0.40	81 mm	0.50	0.1380
4	3.40	1.77	81 mm	0.50	0.1380
5	3.30	3.20	8# shot	0.91	0.0780
6	1.50	3.30	8# shot	0.20	0.0780
7	–0.80	3.50	8# shot	0.20	0.0780
8	–0.70	1.50	M75	0.15	0.1380
9	1.31	1.71	60 mm	0.25	0.0866

It was estimated that the recovered x and y locations of both TESSA and the buried UXO had small systematic and random errors accumulatively totaling 0.25 m. Therefore, the x and y positions of the dipoles were adjusted within this bound to match the positions of the anomalies. It is encouraging that positional matches were established without exceeding the error bound.

Because the UXO targets were degaussed before being buried, we assumed that no remanent magnetism existed, only induced magnetism; therefore, the dipole moment direction was held constant, in alignment with the Earth's field at declination 0 and inclination 58.7 degrees. Although this assumption could be in error by 20 to 30 degrees in both declination and inclination, it suits the qualitative nature of this application, especially considering that the position of the determinant anomaly is not affected much by the moment direction.

There were no independent data available to evaluate the moment magnitudes of the buried dipoles. Consequently, we chose to adjust the moment magnitude of the central dipole so that the peak value of the modeled determinant (fig. 11) matched the peak value of the measured determinant (fig. 10). The moment magnitudes of the flanking dipoles were similarly adjusted to match the flanks of their corresponding anomalies (their peaks were beyond the high-density grid boundaries). It is again encouraging that the resulting moment magnitudes were of reasonable values for all of the targets.

Map views of the collocated TMGS data (physical) and modeled results for the high-density grid can be seen in figures 12 and 13. The similarities between the physical and modeled results are striking, particularly of the central 60-mm UXO (ID 9). In addition, the dipole moments are reasonable. Values around the perimeter of the physical data, while reasonable, could be subject to significant edge effects. Therefore, the fact that any of them have similarities to the model gives further confidence in the TMGS. The origin of a huge negative anomaly in the southeast corner of the physical grid is not altogether clear. However, it is likely due to a real source, possibly clutter, because edge effects around other parts of the grid do not lead to such intense anomalies.

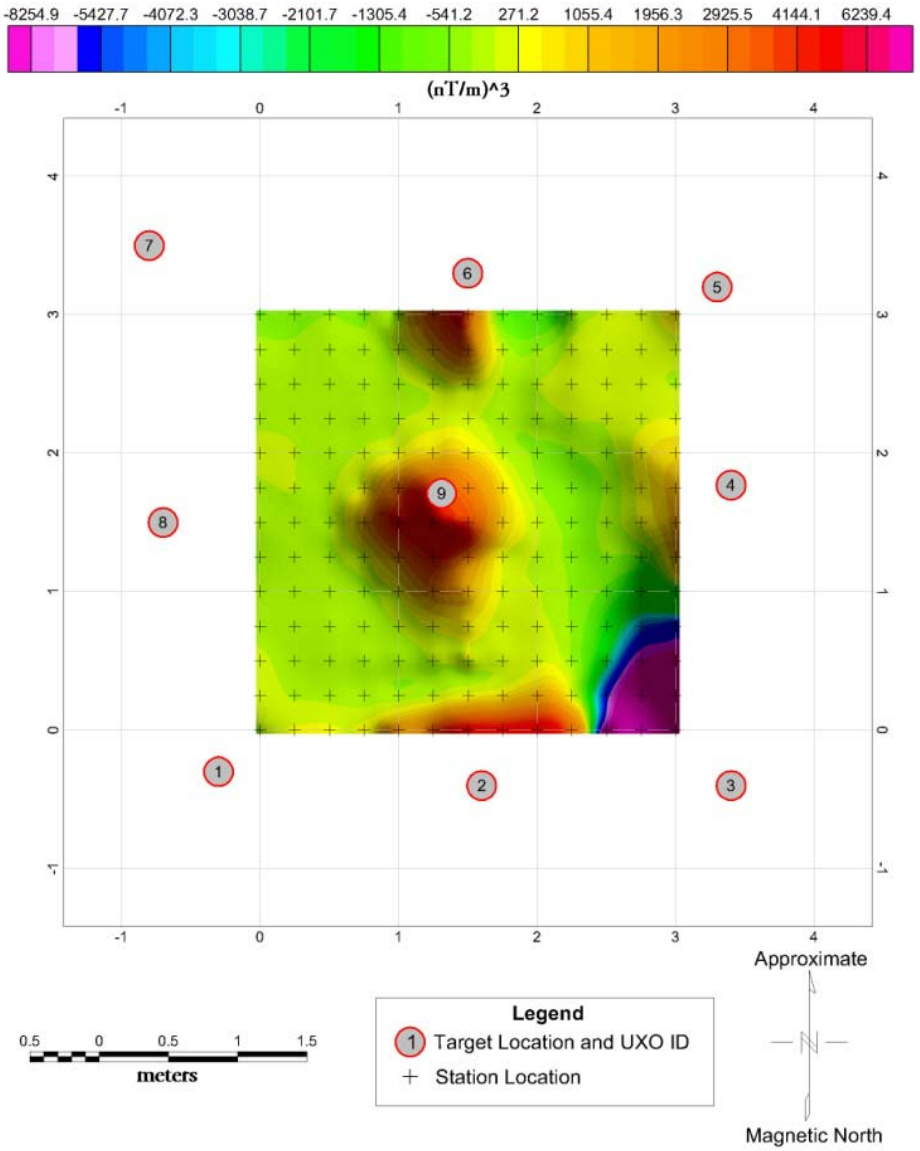

Figure 12. Determinant plot of physical data using the same color scale as the modeled data seen in figure 13. The UXO IDs correspond to the data presented in table 11.

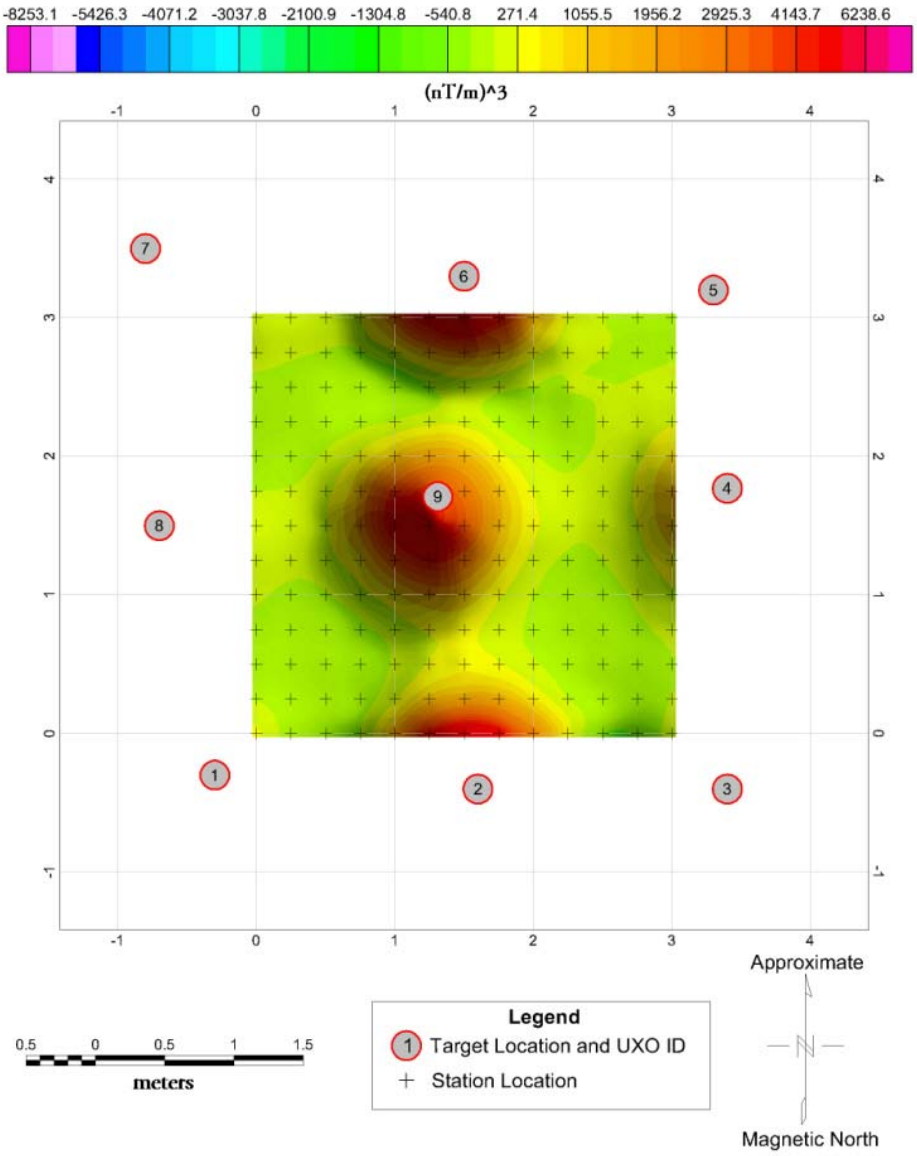

Figure 13. Determinant plot of modeled data using the same color scale as the physical data seen in figure 11. The UXO IDs correspond to the data presented in table 11.

Modeled values are plotted against physical values in figure 14, and table 12 shows statistics for the residual of the modeled and physical data. Essentially, these statistics represent the deviation of the model values from the ideal value represented by the fuchsia line drawn in the figure 14 cross plot. These statistics are skewed both by edge effects (as described in "Gradient Collocation") and by the fact that no attempt was made to model the clutter in the southeast corner.

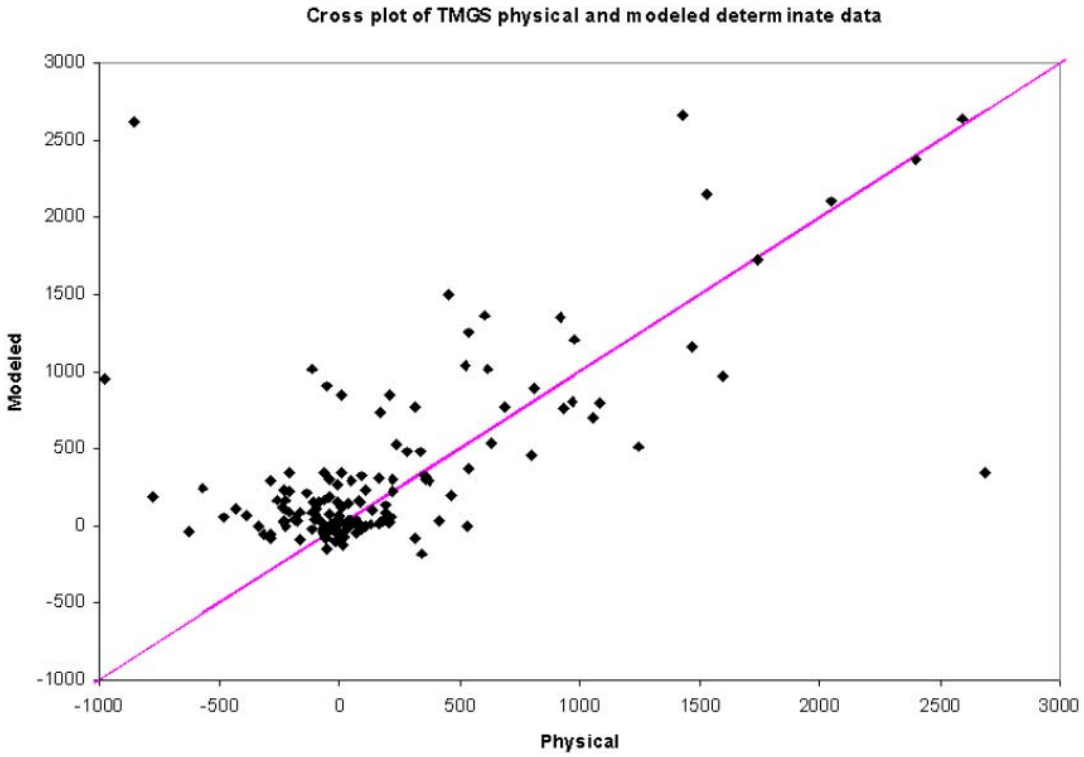

Figure 14. Cross plot of modeled versus physical magnetic tensor determinant data. The statistics for the deviation of the model from the ideal data line drawn in fuchsia can be seen in table 12. This plot is skewed by edge effects and clutter in the southeast corner.

Table 12. Statistics for the model and physical data residual. These statistics are skewed by edge effects and clutter in the southeast corner.

Modeling residual statistics	
Geometric mean	95.15
Standard error	6.75
Standard deviation	572.39
Mean	–154.93
Median	–64.87
Mode	15.5

Conclusions

The similarity of the physical (measured) and modeled results indicates that the reduction process is producing real tensor data. This preliminary analysis is convincing for two compelling reasons. First, the determinant uses all nine tensor components, making its value representative of the whole tensor. Second, the physical and modeled invariant maps are quite similar, which means that the system consistently produced realistic values under a large variety of target-field conditions.

Several stages of the data reduction are critical. If any stage is missing or its coefficients are inaccurate, the resultant tensor map will be incomprehensible. This is in contrast to a typical scalar magnetics survey in which the basic anomalies are usually visible from the raw data and simply improve as reductions are performed. The TMGS processing stages are analogous to a keyed lock—if any tumbler is out of place, the lock will not open. This observation is well illustrated in figure 7, which shows how the final processed map would have appeared if all but the last two reduction stages were performed. The map is completely devoid of any hint that the reduction is moving toward a reasonable result.

Future work on our system includes changing the geometry and reducing the size of the sensor array to handle field curvature and modifying the data-acquisition systems to facilitate data collection on the fly. We expect further research on the reduction process to validate proposed tracking algorithms and to allow an abbreviated spin calibration. We are also studying tensors and tensor invariants for detecting, locating, and modeling sources.

Acknowledgments

This research was supported by the U.S. Department of Defense through the Strategic Environmental Research and Development Program (SERDP). We acknowledge YPG personnel for facilitating our work at the Standardized UXO Test Site and Professor Yaoguo Li of the Colorado School of Mines for providing consultation.

References Cited

Acuna, M.H., Scearce, C.S., Seek, J.B., and Scheifele, J., 1978, The MAGSAT vector magnetometer—A precision fluxgate magnetometer for the measurement of the geomagnetic field: Greenbelt, Md., National Aeronautics and Space Administration Technical Memorandum 79656, 18 p.

Billings, S.D., 2004. Discrimination and classification of buried unexploded ordnance using magnetometry: IEEE Transactions of Geoscience and Remote Sensing, v. 42, p. 1241–1251.

Bracken, R.E., Grover, T.P., and Puniwai, G., 1998, Development and testing of a tensor magnetic gradiometer system with trial monitoring near the Kilauea Volcano, Hawaii: U.S. Geological Survey Open-File Report 98–773, 163 p.

Bracken, R.E., Smith, D.V., and Brown, P.J., 2005, Calibrating a tensor magnetic gradiometer using spin data: U.S. Geological Survey Scientific Investigations Report 2005–5045, 5 p., available online at URL <http://pubs.usgs.gov/sir/2005/5045/>.

Kaufman, A.A., 1992, Geophysical field theory and method—Gravitational, electric and magnetic fields: San Diego, Academic Press, 581 p.

Narod, B.B., 1987, Ring core fluxgate magnetometers for use as observatory variometers [abs.]: International Union of Geodesy and Geophysics 19th General Assembly, Abstracts, v. 2, no. GA5.3–3, 673 p.

Pedersen, L.B., and Rasmussen, T.M., 1990, The gradient tensor of potential field anomalies—Some implications on data collection and data processing of maps: Geophysics, v. 55, no. 12, p. 1558–1566.

Smith, D.V., and Bracken, R.E., 2004, Field experiments with the magnetic gradiometer system at Yuma Proving Ground, Arizona, *in* Proceedings of the Symposium on the Application of Geophysics to Engineering and Environmental Problems. (SAGEEP), February 2004.

Wynn, W.M., Frahm, C.P., Carroll, P.J., Clark, R.H., Wellhoner, J., and Wynn, M.J., 1975, Advanced superconducting gradiometer/magnetometer arrays and a novel signal processing technique: IEEE Transactions on Magnetics, v. MAG–11, no. 2, p. 701–707.

Zlotnicki, J., and Le Mouel, J.L., 1988, Volcanomagnetic effects observed on Piton de la Fournaise volcano (Reunion Island), 1985–1987: Journal of Geophysical Research, v. 93, no. B8, p. 9157–9171.

Appendix A – Fortran routine called s_ab2h.f that applies the bin-size, axis polynomial, orthogonality, and attitude coefficients to basic TMGS analog and bin data.

```
C
C_____________________________________________________________________
C
C     SUBROUTINE  S _ A B 2 H
C_____________________________________________________________________
C
C SUBROUTINE S_AB2H RETURNS THE MAGNETIC FIELD COMPONENTS AND A
C GRADIENT TENSOR IN A FIXED REFERENCE FRAME USING DATA AND
C COEFFICIENTS FROM THE USGS TMGS PROTOTYPE SYSTEM.
C
C THIS SUBROUTINE IS DESIGNED PRIMARILY TO SHOW HOW THE
C COEFFICIENTS DERIVED FROM THE YUMA, 13MAR03 SPIN CALIBRATION
C ARE TO BE APPLIED TO THE RAW TMGS DATA.  THE PRELIMINARY
C COEFFICIENTS MAY BE FOUND IN AN ASCII TEXT FILE CALLED:
C
C            "tmgs_coefs_n0430_yuma_prelim.txt".
C
C
C INPUT ARGUMENTS (SIGNALS)
C   VANA   - REAL*8.  ARRAY OF DIMENSIONS (3,4) CONTAINING THE
C            ANALOG FIELD MEASUREMENTS <VOLTS> FROM THE 3 AXES OF
C            THE 4 MAGNETOMETERS.  ROWS 1,2,3 CORRESPOND TO THE
C            X,Y,Z AXES AND COLUMNS 1,2,3,4 CORRESPOND TO THE
C            MAGNETOMETER NUMBERS.  IT IS EXPECTED THAT THESE
C            NUMBERS WILL HAVE BEEN CORRECTED FOR SPIKES AND
C            NOISE, AND THAT ANALOG FILTER RESPONSES WILL HAVE
C            BEEN DECONVOLVED (PARTICULARLY IMPORTANT IMMEDIATELY
C            AFTER A BIN STEP.) PRIOR TO CALLING THIS SUBROUTINE.
C            TYPICALLY, THESE SIGNALS WILL RANGE FROM +-5 BUT MAY
C            RAIL AT +-6.55 VOLTS.  THESE SIGNALS TRANSLATE TO
C            MAGNETIC FIELD NOMINALLY AT ABOUT 100 nT/VOLT (SEE
C            ARGUMENT CANA BELOW).
C   VBIN   - REAL*8.  ARRAY OF DIMENSIONS (3,4) CONTAINING THE
C            BIN NUMBERS <BIN#> FROM THE 3 AXES OF THE 4
C            MAGNETOMETERS.  ROWS 1,2,3 CORRESPOND TO X,Y,Z AXES
C            AND COLUMNS 1,2,3,4 CORRESPOND TO THE MAGNETOMETER
C            NUMBERS.  IT IS POSSIBLE TO HAVE CORRECTED THESE
C            NUMBERS FOR BIN-CURRENT VARIANCES AND THEREFORE THEY
C            ARE NOT NECESSARILY INTEGERS.  TYPICALLY, BIN
C            NUMBERS WILL RANGE FROM +-150 BUT MAY RAIL AT +-255.
C            BIN NUMBERS INDICATE THE AMOUNT OF OFFSET IN THE
C            ANALOG FIELD MEASUREMENT VOLTAGE AND TRANSLATE TO
C            VOLTS NOMINALLY AT ABOUT 5.0 VOLTS/BIN# FOR MAGS 1
C            AND 2 AND 3.3 VOLTS/BIN FOR MAGS 3 AND 4.  (SEE
C            ARGUMENT CBIN BELOW).
C
C INPUT ARGUMENTS (COEFFICIENTS)
C   CBIN   - REAL*8.  ARRAY OF DIMENSIONS (3,4) CONTAINING THE
C            AVERAGE BIN SIZES (S) (VOLTS/BIN#).  ROWS 1,2,3
C            CORRESPOND TO X,Y,Z AXES AND COLUMNS 1,2,3,4
C            CORRESPOND TO THE MAGNETOMETER NUMBERS.  TYPICALLY,
```

```
C            FOR MAGS 1 AND 2, CBIN IS ABOUT 5.0 AND
C            FOR MAGS 3 AND 4 IT'S ABOUT 3.3 VOLTS/BIN#.
C   CANA   - REAL*8.  ARRAY OF DIMENSIONS (4,3,4) CONTAINING THE
C            POLYNOMIAL COEFFICIENTS (A,B,C,D) THAT TRANSLATE
C            ANALOG VOLTAGE TO MAGNETIC FIELD <nT/VOLT^3,
C            nT/VOLT^2, nT/VOLT, nT>.  ROWS 1,2,3,4 CORRESPOND TO
C            THE 3RD ORDER, 2ND ORDER, LINEAR, AND CONSTANT TERMS
C            RESPECTIVELY OF THE POLYNOMIAL.  COLUMNS 1,2,3
C            CORRESPOND TO X,Y,Z AXES AND LEVELS 1,2,3,4
C            CORRESPOND TO THE MAGNETOMETER NUMBERS.  TYPICALLY,
C            THE 3RD ORDER TERM IS EXTREMELY SMALL, THE 2ND
C            ORDER TERM IS VERY SMALL, THE LINEAR TERM IS NEAR
C            100, AND THE CONSTANT TERM IS SMALL.  THESE
C            COEFFICIENTS ARE AUGMENTED BY THE SCALE DIVISOR THAT
C            WAS APPLIED IN THEIR DERIVATION (SEE ARGUMENT
C            SCALE).
C   SCALE  - REAL*8.  SCALAR NUMBER (SCALE) THAT WAS USED DURING
C            DERIVATION OF THE 3RD-ORDER-POLYNOMIAL COEFFICIENTS
C            DESCRIBED IN ARGUMENT CANA.  THIS SUBROUTINE WILL
C            CORRECTLY APPLY SCALE TO THE COEFFICIENTS.  BUT IF
C            IT IS DESIRED TO APPLY IT BEFORE THE SUBROUTINE
C            CALL, SIMPLY DIVIDE THE 3RD-ORDER TERM BY SCALE^2,
C            DIVIDE THE SECOND ORDER TERM BY SCALE, AND MULTIPLY
C            THE CONSTANT TERM BY SCALE; THEN SET SCALE, ITSELF,
C            EQUAL TO 1.
C   CORT   - REAL*8.  ARRAY OF DIMENSIONS (3,4) CONTAINING THE
C            ORTHOGONALITY CORRECTION ANGLES (DEGREES).  ROWS
C            1,2,3 CORRESPOND TO ANGLES (ALP), (BET), (GAM), AND
C            COLUMNS 1,2,3,4 CORRESPOND TO THE MAGNETOMETER
C            NUMBERS.  ALPHA IS THE ANGLE BETWEEN THE X AND Y
C            AXIS.  BETA IS THE ANGLE BETWEEN THE Y AND Z AXIS.
C            AND, GAMMA IS THE ANGLE BETWEEN THE X AND Z AXIS.
C            TYPICALLY, EACH OF THESE ANGLES VARIES FROM 88 TO 92
C            DEGREES.
C   CATT   - REAL*8.  ARRAY OF DIMENSIONS (3,4) CONTAINING THE
C            ATTITUDES (DEGREES) OF THE MAGS RELATIVE TO MAG1.
C            ROWS 1,2,3 CORRESPOND TO ANGLES (DEL), (EPS), (ZET),
C            AND COLUMNS 1,2,3,4 CORRESPOND TO THE MAGNETOMETER
C            NUMBERS.  IN TRANSFORMING FROM EACH MAGNETOMETER'S
C            PHYSICAL ATTITUDE TO THE MAG1 ATTITUDE, THERE ARE 3
C            ROTATIONS.  THE POSITIVE SENSE IS ALWAYS CLOCKWISE
C            ABOUT THE ROTATION AXIS AS VIEWED FROM THE ORIGIN.
C            DELTA IS THE FIRST ROTATION ANGLE AND PROCEEDS ABOUT
C            THE Z''' AXIS.  EPSILON IS THE SECOND ROTATION ANGLE
C            AND PROCEEDS ABOUT THE Y'' AXIS.  ZETA IS THE THIRD
C            ROTATION ANGLE AND PROCEEDS ABOUT THE Z' AXIS.
C            THEREFORE, THE UNPRIMED SYSTEM IS THE MAG1 ATTITUDE.
C            TYPICALLY, EACH OF THESE ANGLES VARIES BY +-2
C            DEGREES ABOUT THE IDEAL.  THE IDEAL ANGLES ARE AS
C            FOLLOWS:
C
C            ROTATION  MAG1       MAG2       MAG3       MAG4
C              DEL        0          0       +120       -120
C              EPS        0       -109.471   -109.471   -109.471
C              ZET        0        180        +60        -60
C
C
```

```
C OUTPUT ARGUMENTS:
C   HFLD   - REAL*8.  ARRAY OF DIMENSIONS (3,4) CONTAINING THE
C            MAGNETIC FIELD COMPONENTS (nT).  ROWS 1,2,3
C            CORRESPOND TO X,Y,Z AXES AND COLUMNS 1,2,3,4
C            CORRESPOND TO THE MAGNETOMETER NUMBERS.  THE FIELDS
C            ARE CALIBRATED, THE AXES ARE ORTHOGONAL, AND THE
C            MAGNETOMETERS ARE IN THE MAG1 COMMON REFERENCE
C            FRAME.  THE ARRAY IS LAYED OUT PICTORIALLY AS
C            FOLLOWS:
C
C                 X1 X2 X3 X4
C                 Y1 Y2 Y3 Y4
C                 Z1 Z2 Z3 Z4
C
C   GTSR   - REAL*8.  ARRAY OF DIMENSIONS (3,3) CONTAINING THE
C            MAGNETIC GRADIENT TENSOR (nT/m) DERIVED FROM HFLD,
C            ASSUMING A TETRAHEDRAL CONFIGURATION OF THE 4
C            MAGNETOMETERS WITH 0.97 METERS DISTANCE BETWEEN
C            CENTERS.  WITH 4 SENSORS, A DIRECT DERIVATION OF
C            EACH OF THE 9 COMPONENTS OF THE TENSOR IS AVAILABLE.
C            HOWEVER, IF A) THE FIELD IS STATIC, B) ALL OF THE
C            GRADIENTS ARE CONSTANT WITHIN THE VOLUME OF TESSA,
C            AND C) THERE IS NO MEASUREMENT NOISE, THEN THE
C            TENSOR WILL BE TRACELESS AND SYMMETRIC, HAVING ONLY
C            5 INDEPENDENT COMPONENTS.  THEREFORE, TO THE DEGREE
C            THAT IT IS NOT TRACELESS AND SYMMETRIC, ONE OR MORE
C            OF THESE CONDITIONS HAS NOT BEEN REACHED.  THE ARRAY
C            IS LAYED OUT PICTORIALLY AS FOLLOWS:
C
C                 Gxx Gxy Gxz
C                 Gyx Gyy Gyz
C                 Gzx Gzy Gzz
C
C                    WHERE:
C
C                    Gij = dHi/dj = gtsr(i,j)
C
C
C SUBROUTINE S_AB2H WRITTEN BY ROB BRACKEN, USGS.
C FORTRAN 77, HP FORTRAN/9000, HP-UX RELEASE 11.0
C VERSION 1.0, 20030430 ( ORIGINAL CODE ).
C
C
      subroutine s_ab2h(vana,vbin, cbin,cana,scale,cort,catt
     &                 ,hfld,gtsr )
C
C
C DECLARATIONS
C
C     INPUT ARGUMENTS (SIGNALS)
      real*8 vana(3,4),vbin(3,4)
C
C     INPUT ARGUMENTS (COEFFICIENTS)
      real*8 cbin(3,4),cana(4,3,4),scale,cort(3,4),catt(3,4)
C
C     OUTPUT ARGUMENTS (FIELDS AND TENSOR)
      real*8 hfld(3,4),gtsr(3,3)
```

```
C
C
C     INTERNAL VARIABLES
C
C     AXIS VOLTAGE RECONSTRUCTION
      real*8 va(3,4)
C
C     FIELD CORRECTION
      real*8 hf(3,4)
C
C     ORTHOGONALITY CORRECTION
      real*8 hfl(3,4)
      real*8 alp,bet,gam
      real*8 calp,salp, cbet, cgam
      real*8 coseta
C
C     ATTITUDE ROTATION TO MAG1 REFERENCE FRAME
      real*8 del,eps,zet
      real*8 cdel,sdel, ceps,seps, czet,szet
C
C     GRADIENT TENSOR CALCULATIONS
      real*8 edge, face, cent
      real*8 edge2,face3,cent4
C
C
C RECONSTRUCT AXIS VOLTAGE FROM ANALOG VOLTAGE AND BIN NUMBER
C
      do k=1,4
        do j=1,3
          va(j,k)=
     &             vana(j,k)
     &            +vbin(j,k) * cbin(j,k)
        enddo
      enddo
C
C
C CONVERT AXIS VOLTAGE TO CORRECTED MAGNETIC FIELD (nT)
C
      do k=1,4
        do j=1,3
          hf(j,k)=
     &              1         * cana(4,j,k) * scale
     &            +va(j,k)    * cana(3,j,k) *     1
     &            +va(j,k)**2 * cana(2,j,k) / scale
     &            +va(j,k)**3 * cana(1,j,k) / scale**2
        enddo
      enddo
C
C
C APPLY ORTHOGONALITY CORRECTION
C
      do k=1,4
C
C       X TO Y ANGLE
        alp=cort(1,k)
        calp=dcosd(alp)
        salp=dsind(alp)
```

```
C
C       Y TO Z ANGLE
        bet=cort(2,k)
        cbet=dcosd(bet)
C
C       X TO Z ANGLE
        gam=cort(3,k)
        cgam=dcosd(gam)
C
C       COSINE OF THE ANGLE BETWEEN Z AND Z-PRIME
        coseta=dsqrt(1.d0-cbet**2-cgam**2)
C
C       X-AXIS CANNOT "MOVE"
        hfl(1,k)=
     &           hf(1,k)
C
C       Y-AXIS CAN "MOVE" ONLY IN THE X-Y PLANE
        hfl(2,k)=
     &        ( -hf(1,k)*(     calp          )
     &          +hf(2,k)                       ) / salp
C
C       Z-AXIS CAN "MOVE" ANYWHERE
        hfl(3,k)=
     &        (  hf(1,k)*(cbet*calp/salp-cgam)
     &          -hf(2,k)*(cbet     /salp     )
     &          +hf(3,k)                       ) / coseta
C
      enddo
C
C
C APPLY ATTITUDE XFRM (ROTATION) TO COMMON (MAG1) REFERENCE FRAME
C
      do k=1,4
C
C       ROTATION 1 IS ABOUT Z'''
        del=catt(1,k)
        cdel=dcosd(del)
        sdel=dsind(del)
C
C       ROTATION 2 IS ABOUT Y''
        eps=catt(2,k)
        ceps=dcosd(eps)
        seps=dsind(eps)
C
C       ROTATION 3 IS ABOUT Z'
        zet=catt(3,k)
        czet=dcosd(zet)
        szet=dsind(zet)
C
C       FIND THE ROTATED COMPONENTS
        hfld(1,k)=
     &           hfl(1,k)*( czet*ceps*cdel-szet*sdel )
     &          +hfl(2,k)*( czet*ceps*sdel+szet*cdel )
     &          +hfl(3,k)*(-czet*seps                )
        hfld(2,k)=
     &           hfl(1,k)*(-szet*ceps*cdel-czet*sdel )
     &          +hfl(2,k)*(-szet*ceps*sdel+czet*cdel )
```

```
     &          +hfl(3,k)*( szet*seps               )
        hfld(3,k)=
     &           hfl(1,k)*(      seps*cdel          )
     &          +hfl(2,k)*(      seps*sdel          )
     &          +hfl(3,k)*(      ceps               )
      enddo
C
C
C FIND GRAD TENSOR WHERE:  gtsr(i,j) = Gij = dHi/dj
C
C     Note:  With 4 sensors, a direct measurement of all 9
C            components of the tensor is available.  However, if
C            a) the field is static, b) all of the gradients are
C            constant within the volume of TESSA, and c) there is
C            no measurement noise, then the tensor will be
C            traceless and symmetric, having only 5 independent
C            components.  Therefore, to the degree that it is not
C            traceless and symmetric, one or more of these
C            conditions has not been reached.
c
      call s_h2g(hfld, gtsr)
C
C
C EXIT PROCEDURE
C
  990 return
      end
```